# Abundance, horizontal and vertical distribution of epipelagic ctenophores and scyphomedusae in the northern Bering Sea in summer 2017 and 2018: quantification by underwater video imaging analysis

Marie Maekakuchi[a,+], Kohei Matsuno[a,b], Jun Yamamoto[c], Yoshiyuki Abe[d], Atsushi Yamaguchi[a,b]*

[a] Graduate School of Fisheries Sciences, Hokkaido University, 3-1-1 Minato-cho, Hakodate, Hokkaido, 041-8611, Japan

[b] Arctic Research Centre, Hokkaido University, Kita-21 Nishi-11 Kita-ku, Sapporo, Hokkaido, 001-0021, Japan

[c] Field Science Centre for Northern Biosphere, Hokkaido University, 3-1-1 Minato-cho, Hakodate, Hokkaido, 041-8611, Japan

[d] URA Station, Hokkaido University, Kita-21 Nishi-10 Kita-ku, Sapporo, Hokkaido, 001-0021, Japan

[+] Present address; APA Hotel and Resorts Co. Ltd., Akasaka 3-2-3, Minato, Tokyo, 107-0052, Japan

* Corresponding author. E-mail address: a-yama@fish.hokudai.ac.jp (A. Yamaguchi).

**Abstract**

We examined the abundance and horizontal and vertical distributions of epipelagic ctenophores and scyphomedusae in the northern Bering Sea using an underwater video camera during July of 2017 and 2018. The effects of environmental and biological parameters on the distribution of these species were evaluated by generalized additive modelling (GAM). In 2017, the dominant ctenophore, *Bolinopsis infundibulum*, was mainly distributed in the north and west of St. Lawrence Island (SLI), and their vertical distribution varied with the region but not by the time of day. We found that *B. infundibulum* was distributed in the upper pycnocline north of SLI, but below the pycnocline west of SLI. Biological interactions with other gelatinous zooplankton may explain these regional differences in vertical distribution; GAM analysis revealed a negative interaction between *B. infundibulum* and the large scyphomedusa, *Chrysaora melanaster,* which occurred in the upper layer in the west of SLI. *B. infundibulum* may avoid that layer to reduce feeding competition. For the ctenophore, *Beroe* sp., vertical and horizontal distributions were similar to those of *B. infundibulum,* and GAM analysis also revealed a positive interaction for both species. As *B. infundibulum* is an important prey of *Beroe* sp., a prey-predator interaction may result from their similar horizontal and vertical distributions. Standing stocks of epipelagic ctenophores and scyphomedusae in 2018 were low compared to those in 2017, by a factor of 1/20 (*C. melanaster*) and1/90 (*Beroe* sp.). This might be due to annual differences in water mass in this region, in that

the thermal conditions characterized by a high abundance of the dominant *B. infundibulum* in 2017 (<2 and >8°C) were absent in 2018. As this drastic decrease in standing stock in 2018 was apparent for both ctenophores and scyphomedusae, food availability was hypothesized to be poor that year.

**Keywords:**

Ctenophores, Scyphomedusae, Northern Bering Sea, Vertical distribution, Horizontal distribution, Imaging analysis

45 **1. Introduction**

46 Recently, increases in the abundance of large ctenophores and scyphomedusae have been
47 reported in various oceans worldwide, likely due to human alternation of marine environments and
48 climate change (Purcell et al., 2007; Condon et al., 2013; Duarte et al., 2013). The main food
49 sources of ctenophores and scyphomedusae in higher latitudes are mesozooplankton, especially
50 copepods (Brodeur et al., 2002; Purcell et al., 2010). Ctenophores and scyphomedusae are thus
51 competitors of the planktivorous fishes, and also act as predators upon larval fishes; thus, the
52 abundance of large gelatinous zooplankton can have a great effect on fish stocks (Brodeur et al.,
53 2002; Purcell et al., 2007; Robinson et al., 2014). As large gelatinous zooplankton are composed
54 mainly of water and require less organic material for their body composition, they can respond to
55 environmental changes more rapidly than crustacean zooplankton, and their biomass can vary
56 dramatically between years (Falkenhaug, 1996; Brodeur et al., 2008).

57 The northern Bering Sea, the target area of the present study, is a transit region for the
58 warmer waters of southern origin (Alaskan Coastal Water, Bering Shelf Water, Anadyr Water),
59 which intrude into the western Arctic Ocean (Shimada et al., 2006; Sasaki et al., 2016; Danielson et
60 al., 2017). A polynya forms south of St. Lawrence Island (SLI), the largest island in this region,
61 and is characterized as being ice-free, even in winter (Grebmeier and Cooper, 1995). Recently, a
62 drastic decrease in the ice-covered area and an early ice retreat in the northern Bering Sea has been

63 reported (Comiso et al., 2008; Parkinson and Comiso, 2013; Stabeno and Bell, 2019).
64 Additionally, changes in zooplankton biomass, a northern shift of the fish community, and a mass
65 mortality of seabirds occurred during the winter of 2017/2018 and spring/summer of 2018
66 (Cornwall, 2019; Duffy-Anderson et al., 2019; Huntington et al., 2020). Under conditions of
67 greater variability in the environment and marine ecosystem, the amount and distribution of
68 ctenophores and scyphomedusae were also expected to change. However, ecological information on
69 these species is presently scarce for this region.
70 The methods used to quantify ctenophores and scyphomedusae have several limitations
71 (Graham et al., 2003, Uye et al., 2017). Traditional sampling using a plankton net tow is hampered
72 by patchy spatio-temporal distributions, relatively large body size, low abundance, and net
73 avoidance, leading to inevitable underestimation of their biomass and species diversity (Youngbluth
74 and Båmstedt, 2001; Graham et al., 2003; Raskoff et al., 2005; Uye et al., 2017). The fragile
75 bodies of ctenophores and scyphomedusae are also heavily damaged by net towing (Graham et al.,
76 2003; Raskoff et al., 2005: Uye et al., 2017). Large-volume trawl nets have been used; however,
77 using these nets requires large effort and cost compared to plankton sampling. Moreover, changes
78 in the mouth area and collection efficiency varies with mesh size and towing speed. These nets
79 cause serious damage to the fragile bodies of gelatinous zooplankton, making quantitative collection
80 difficult for ctenophores and scyphomedusae (Graham et al., 2003, Uye et al., 2017). To overcome

these problems in the quantification of ctenophores and scyphomedusae, alternative non-capture methods such as sonar cameras (Han and Uye, 2009), video cameras using a Remotely Operated Vehicle (Båmstedt and Martinussen, 2015), and visual monitoring using ships and airplanes (Purcell et al., 2000) have been used.

In the Bering Sea, Brodeur et al. (2017) reported horizontal distributions, and seasonal and annual changes in ctenophores and scyphomedusae based on data collected by trawl nets, although there was the paucity of data for the northern Bering Sea. The vertical distributions of ctenophores and scyphomedusae in the southeastern Bering Sea have been observed using a video camera mounted on an ROV (Brodeur, 1998; Brodeur et al., 2002). Annual variations in the biomass of the large scyphomedusa, *Chrysaora melanaster*, over the southeastern Bering Sea shelf has previously been analysed using Generalized Additive Models (GAM) to explore which environmental variables might explain the variability (Brodeur et al., 2008). Although the northern Bering Sea is characterized by large interannual changes in the ice-covered area and timing of the ice retreat, few studies have investigated interannual changes in ctenophores and scyphomedusae in this region.

In the present study, we quantified the horizontal and vertical distributions, and annual changes in the abundances of ctenophores and scyphomedusae using an underwater video camera in the northern Bering Sea during the summers of 2017 and 2018. Interactions among vertical, horizontal, and annual changes in the abundance of ctenophores and scyphomedusae were assessed

with environmental parameters (depth, temperature, salinity, diel period, year, and location relative to the pycnocline) and biological parameters (mesozooplankton biomass, other species of ctenophores and scyphomedusae) by GAM analysis.

## 2. Material and methods

### *2.1. Field observation*

Imaging data for ctenophores and scyphomedusae were collected by vertical casts of a frame camera at 21 (2017) and 14 (2018) stations located between 63°00'–66°44'N and 166°30'–174°50'W in the northern Bering Sea. These sampling stations were occupied by the T/S *Oshoro-Maru* during 9–22 July 2017 and 2–12 July 2018 (Fig. 1). Imaging data down to 50 m were collected by dead-slow (0.1 m $s^{-1}$) vertical deployment of an underwater video camera (Marine Arkas, Kowa Co. Ltd.) mounted within a stainless frame of 1.0 × 1.0 m bottom and 1.5 m depth (Fig. 2B). A charge-coupled device (CCD) camera (NTSC PA-290) was equipped with a *f*2.9 lens that had 0.035 lux light sensitivity. The final resolution of each digital frame was 768 (horizontal) by 494 (vertical) pixels. The *in situ* images were monitored from the ship. To evaluate diel changes in vertical distribution, observations were made at 1 h intervals at one station (St. 10) during 19:40–7:10, 13–14 July 2017 (total number of samples = 11) (Appendix A). Observations were made both day and night at three additional stations (St. 14, 20, and 23) in 2017. At each station, temperature and

117 salinity were measured using a Conductivity Temperature Depth (CTD) sensor (SBE911, Sea-Bird
118 Electronics, Inc.). To evaluate mesozooplankton biomass, a vertically-stratified tow of a 60 cm
119 opening-closing net (mesh size: 100 μm) (Kawamura, 1989) was conducted from the sea-surface to
120 the thermocline, and from the thermocline to near-bottom. Mesozooplankton samples were
121 preserved in 5% (v/v) borax-buffered formalin seawater.
122 The underwater camera (Marine Arkas, Kowa Co. Ltd.) was equipped with two halogen
123 lights (JCD100V-150W) with 150W and 3300 lumen luminous flux and a pressure-depth sensor
124 (model P193-010-45, SENSIT., Co. Ltd., Hampshire, UK) with a precision of ±0.25%FS. A
125 picture of the frame camera is presented in Fig. 2B. Using the bottom observation frame as a
126 guide, the camera was able to image an observational area of 1.2 × 0.8 m (Fig. 2B, C). On the side
127 of the frame, a current fin (0.8 × 0.3 m) was attached so that the horizontal current was flowing in
128 one direction along the diagonal of the bottom observation frame. Sinkers (20 kg each) were set at
129 the four corners of the frame. We measured the wire angle, and, because of the heavy weight of the
130 camera and frame, the angles were less than 5˚ at each cast. Underwater videos were transferred
131 on-board through a tether cable and recorded using an HDD and DVD recorder (Toshiba RD-X4).
132 The recording method was MPEG2. The depth data were displayed on a captured image and were
133 recorded using video imaging data. For examples of the video images, see video supplemental
134 materials captured for Cast 14 at St. 10 on 14 July 2014 (Video 1) and for Cast 27 at St. 19 on 19

July 2017.

*2.2. Quantification of ctenophores and scyphomedusae*

In the laboratory on land, all ctenophores and scyphomedusae within the observation frame (0.8 m x 1.2 m) were identified and counted in 2 m vertical intervals from the recorded video. As the frame camera was towed at a speed of 0.1 m $s^{-1}$, video images obtained at 2 m depth intervals corresponded to 20 s (= 2.0/0.1). Depth data were expressed with 0.1 m accuracy, and the error for estimated depths obtained by the sonar- equipped ship was less than 0.5 m. To evaluate the flow rates of horizontal currents, the diagonal passage time (*Pt*, s) of ctenophores, scyphomedusae and marine snow within the observation field was measured at 10 m intervals. The *Pt* was not varied with the targets. For real images of the video, see video supplemental materials. Note that we measured current speed every 10 m constantly and applied these current data for jellyfishes quantified with 2 m interval.

To calculate individual density, observation volume over 2 m intervals ($V$, $m^3$) was calculated from the following equation (Fig. 2C):

$V = 2 \times 1.2 \times 0.8 \times 20 \times 1/Pt$,

where, $2 \times 1.2 \times 0.8$ is the volume of the observation field (height × width × depth, $m^3$). Thus, $1/Pt$ represents the changes in viewing within 1 s. As a 2 m vertical movement of the video camera

153 required 20 s., "20 × 1/*Pt*" represents the change in view caused by horizontal advection within a 2
154 m observation distance. Swimming speeds of ctenophores and scyphomedusae may also affect
155 their quantification. The swimming speed ($V$: cm $s^{-1}$) of ctenophores is known to be a function of
156 diameter (*Dia*: cm): $V = 0.12 + 0.04\ Dia$ (Cowan and Houde, 1992). If we assume 15-20 cm
157 diameter, the swimming speed of the ctenophore would have been 0.72-0.92 cm $s^{-1}$. From *Pt*, the
158 horizontal current speed was calculated to be ca. 0.5-2.0 m $s^{-1}$. Thus, since horizontal current speed
159 was generally faster than the swimming speed of ctenophores and scyphomedusae, the effect of their
160 swimming speeds on the quantification of their numbers was ignored.
161 Ctenophores and scyphomedusae were quantified for both the descent ($D$) and ascent( $A$)
162 of the tows, and the data from both directions corresponded well ($D = 0.857 \times A$, $r^2 = 0.742$, $\rho$
163 <0.0001, $n = 561$) (Appendix B). Thus, we calculated the mean descent and ascent abundance for
164 each depth. The settling volume for mesozooplankton samples collected by the closing net was
165 measured with 0.1 mL accuracy and expressed as their biovolume biomass (mL $m^{-3}$).
166
167 *2.3. Statistical analysis*
168 To examine diel changes in vertical distribution, the abundances at depths of 10, 25, 50, 75, and 90%
169 ($D_{10\%}$, $D_{25\%}$, $D_{50\%}$, $D_{75\%}$, and $D_{90\%}$, respectively, Pennak, 1943) were calculated for all stations at
170 which day-night observations were made (St. 10, 14, 20, 23, in 2017). To evaluate diel vertical

171 migration, $D_{50\%}$ was compared between the day ($n$=7) and night ($n$=4) using a Mann Whitney U-test
172 at St. 10. For the remaining stations (St. 14, 20, 23) where day and night sampling was conducted,
173 the Kolmogorov-Smirnov test was used to evaluate diel changes in vertical distribution (Sokal and
174 Rohlf, 1995).
175 The effects of environmental and biological parameters on the distribution of ctenophores
176 and scyphomedusae were analysed by GAM. The densities of ctenophores and scyphomedusae
177 were applied as response variables, and environmental and biological parameters, such as
178 hydrography (temperature, salinity), depth, day-night, year, upper/lower pycnocline,
179 mesozooplankton biomass, and the densities of other ctenophores and scyphomedusae were applied
180 as explanatory variables. The pycnocline was defined as the depth at which the seawater density
181 was higher than that at the 5 m depth by 0.1 kg $m^{-3}$ (Danielson et al., 2011). For the GAM analysis,
182 R software with "mgcv" package was used (Wood, 2017).
183
184 **3. Results**
185 *3.1. Hydrography*
186 Cross-sectional distributions of temperature and salinity along each line transect in the northern
187 Bering Sea during 2017 and 2018 are shown in Figs. 3 and 4, respectively. In 2017, water
188 temperatures ranged from -1.26 to 11.6°C and salinities from 30.2 to 32.9 psu, respectively (Fig. 3).

189 In most locations, the upper layer was characterized by warm temperatures and low salinity. No
190 pycnocline developed north of 66°N, near the Bering Strait, whereas a pycnocline was observed
191 around 6–32 m in the western and southern regions of SLI, with substantial differences in
192 temperature between the upper and lower layers. Conversely, in 2018, temperature and salinity
193 ranged from -0.21 to 12.8°C and from 28.3 to 32.9 psu, respectively (Fig. 4). Pycnocline
194 development was much weaker in 2018 than in 2017. The differences in temperature between the
195 upper and lower layers of the pycnocline were smaller in 2018 compared with 2017.
196
197 *3.2. Horizontal distribution of ctenophores and scyphomedusae*
198 Horizontal distributions of ctenophore and scyphomedusa standing stocks (ind. $m^{-2}$) at each
199 sampling station in 2017 and 2018 are shown in Fig. 5. Three taxa of large gelatinous zooplankton
200 were commonly observed: the ctenophores, *Bolinopsis infundibulum* and *Beroe* sp., and the
201 scyphomedusae, *Chrysaora melanaster* (Fig. 2A). Among these, *B. infundibulum* was the most
202 numerous species in both 2017 and 2018. In 2017, the standing stock of *B. infundibulum* was 0–
203 35.6 ind. $m^{-2}$ and was the greatest north and west of SLI. The maximum abundance of *C.*
204 *melanaster* and *Beroe* sp. occurred at 0.689 and 0.567 ind. $m^{-2}$, respectively, and they were abundant
205 west and south of SLI, and north of SLI to the Bering Strait, respectively. In 2018, standing stocks
206 of all species were much lower than those in 2017, and their mean abundance in 2018 was 1/90 (*C.*

207 *melanaster*)–1/20 (*Beroe* sp.) of those in 2017 (Fig. 5).

208

209 *3.3.* Diel changes in the vertical distribution of *Bolinopsis infundibulum*

210 Diel changes in the vertical distribution of *B. infundibulum* were examined at four stations in 2017

211 (Fig. 6). At St. 10, where multiple observations were made, day and night $D_{50\%}$ (mean ± 1 sd) was

212 6.97 ± 4.62 and 1.92 ± 0.32 m, respectively. Although the night $D_{50\%}$ was 5 m shallower than the

213 day $D_{50\%}$, this difference was not significant ($p > 0.05$, *U*-test), suggesting that there was no diel

214 vertical migration (DVM). For the three stations with only one day-night observation (St. 14, 20,

215 23), diel differences were detected at St. 14 and 20 (St. 14: $p < 0.005$, St. 20: $p < 0.001$,

216 Kolmogorov-Smirnov test); however, the diel pattern varied with the station. A nocturnal ascent

217 occurred at St. 14, while a nocturnal descent occurred at St. 20. The diel changes in $D_{50\%}$ were 5.3

218 m (St. 14) and 5.5 m (St. 20). No significant change was detected between the day and night

219 vertical distributions at St. 23 ($p > 0.05$), likely due to the extremely low abundance at that station

220 (Appendix D). For details of each observation, see Appendix C (St. 10) and Appendix D (Sts. 14,

221 20, 23).

222

223 *3.4. Vertical distributions of ctenophores and scyphomedusae*

224 In 2017, the vertical distribution of *B. infundibulum* showed a clear regional pattern (Fig. 7). This

225 species was distributed throughout the water column north of the Bering Strait (St. 1, 5), but was
226 distributed around or below the pycnocline south of the Bering Strait (St. 7, 9). *B. infundibulum*
227 was primarily distributed at shallower depths than the pycnocline north of SLI (St. 12, 13), while a
228 bimodal distribution with peaks in the upper and lower layers of the water column was observed
229 northwest of SLI (St. 16, 18). West of SLI (St. 19, 20, 24), this species was distributed below the
230 pycnocline.

231 In 2017, *C. melanaster* was distributed in a layer shallower than the pycnocline (Fig. 8).
232 In the region west and south of SLI, *C. melanaster* was distributed at shallower depths than the
233 pycnocline with a maximum density at 0.161 ind. $m^{-3}$ (St. 22, 6–8 m) for these regions.

234 *Beroe* sp. were distributed at depths shallower than the pycnocline south of the Bering
235 Strait (St. 6, 9), and both above and below the pycnocline north of SLI (St. 13, 14) (Fig. 9).
236 Conversely, they were distributed entirely below the pycnocline west and south of SLI (St. 18, 20,
237 22, 24).

238

239 *3.5. Interannual changes in ctenophores and scyphomedusae densities*

240 Based on data from all sampling stations, the densities of the most dominant ctenophore (*B.*
241 *infundibulum*) in 2017 and 2018 are shown with the hydrography in Fig. 10. Annual changes were
242 observed between 2017 and 2018, where 2017 showed a bimodal distribution, with high abundances

243 at >8 and <2°C, and low abundance at intermediate temperatures (2–8°C). Conversely, the thermal
244 range available in 2018 was mostly limited to 2–8°C and *B. infundibulum* showed very low densities
245 within these temperature ranges.
246
247 *3.6. GAM Environmental Relationships*
248 In 2018, depth, temperature, salinity, and zooplankton all had significant effects on *B. infundibulum*,
249 which were abundant at night and below the pycnocline; these factors were negatively related to *C.*
250 *melanaster* abundance, and positively related to *Beroe* sp. (Table 1). There was a significant
251 positive relationship between *C. melanaster* abundance and temperature, salinity, and zooplankton
252 biomass, and a negative relationship with *B. infundibulum* abundance. There was a significant
253 relationship between *Beroe* sp. abundance and depth, temperature, salinity, and zooplankton
254 biomass, and a positive interaction with *B. infundibulum* abundance. Smoothing spline regressions
255 between ctenophore and scyphomedusae abundance and environmental parameters with a significant
256 relationship are shown in Fig. 11. The abundance of *B. infundibulum* was high at depths <24 m,
257 temperatures of -1–2, 5.5–7.5, and 9–10°C, salinities of >30.7, 31.8–32.1, and >32.3 psu, and
258 zooplankton biomasses of 0.1–0.6, 1.4–3.0, and 3.4–4.1 mL $m^{-3}$. The abundance of *C. melanaster*
259 was high at temperatures >5.5°C, salinities between 31.0 and 32.4 psu, and zooplankton biomasses
260 of <1.7, and 3.0–4.4 mL $m^{-3}$. The abundance of *Beroe* sp. was high at depths <14 m, temperatures

261 <6.9°C, salinities of <30.4, 30.8–31.3, and 31.7–32.8 psu, and zooplankton biomasses between 0.2–

262 2.1 mL $m^{-3}$.

263

264 **4. Discussion**

265 *4.1. Quantification of ctenophores and scyphomedusae*

266 In the present study, we used an underwater video camera to collect quantitative data on ctenophores

267 and scyphomedusae during day and night, even under dark conditions in the deepest layers using

268 artificial light (3300-lumen luminous flux). Use of an underwater video camera to quantify

269 ctenophores and scyphomedusae has been somewhat limited in past studies by reduced visibility and

270 difficulty quantifying their abundance in high turbidity waters (Honda and Watanabe, 2007; Honda

271 et al., 2016), but we did not encounter high turbidity water in our study region in either year as

272 judged by by using the square frame at the bottom of the frame as a guide.

273 Several metrics have been presented to quantify data on ctenophores and scyphomedusae

274 obtained with an underwater video camera. These include individual number over each observation

275 time within a certain depth range (ind. $min^{-1}$ or ind. $hour^{-1}$) (Toyokawa et al., 2003; Raskoff et al.,

276 2005; Honda and Watanabe, 2007; Raskoff et al., 2010), the individual number observed at each

277 depth (number observed) (Purcell et al., 2010; Båmstedt and Martinussen, 2015), and species

278 composition within the total observed number throughout the water column (%) (Brodeur, 1998).

279 In the present study, we calculated the observed volume by multiplying the observation area (1.2 ×
280 0.8 m) by depth (2 m) and considered the change in view caused by horizontal advection within a 2
281 m observation (Fig. 2C). A similar calculation method has been used in previous studies.
282 Youngbluth and Båmstedt (2001) calculated volume by multiplying the observation area by vertical
283 depth. To account for horizontal advection, the current flow of the water mass was applied (Nogata
284 et al., 2009), and by measuring the horizontal current using a shipboard acoustic Doppler current
285 profiler (ADCP), Honda et al. (2016) were able to calculate volumes considering horizontal
286 advection. On our cruises, horizontal current was also measured by the shipboard ADCP.
287 However, vertical changes in the horizontal current speed were also observed in the present study.
288 Thus, we measured horizontal current speed at depth using the time taken for a particle (e.g. marine
289 snow) to pass through the observation frame at 10 m depth intervals. As we set the current fin for
290 the frame, the horizontal current was flowing diagonally; thus, it was possible to quantify the
291 horizontal current measurements in this study.
292 Båmstedt and Martinussen (2015) reported a maximum density of *B. infundibulum* of 2–5
293 ind. $m^{-3}$ at 0–50 m depths in a western Norwegian fjord. This value corresponds well with the
294 maximum density (3.58 ind. $m^{-3}$) observed in our study. For *C. melanaster*, a maximum density of
295 0.07 ind. $m^{-3}$ has been reported for the southeastern Bering Sea shelf (Brodeur, 1998), whereas in the
296 present study, we observed 0.16 ind. $m^{-3}$. Thus, our use of underwater video to quantify individual

297 density, considering horizontal advection, seems appropriate and comparable to the results of
298 previous studies.
299
300 *4.2. Diel vertical migration of ctenophores and scyphomedusae*
301 For *B. infundibulum*, no diel changes in vertical distribution were observed at two stations (St. 10,
302 23), nocturnal ascent was observed at one station (St. 14), and nocturnal descent was found at one
303 station (St. 20). However, where changes were observed, the diel differences were small (5.3–5.5
304 m). Little information is available regarding the DVM of ctenophores (Vereshchaka, 2002;
305 Haraldsson et al., 2014; Júnior et al., 2015). The absence of DVM in ctenophores has been
306 attributed to their lacking organs that can detect light (Graham et al., 2001). However, it was
307 recently reported that ctenophores may possess an organ capable of detecting light (Haraldsson et al.,
308 2014).
309 The DVM pattern observed for *B. infundibulum* varied with the station, and the magnitude
310 (5.3–5.5 m) was close to the sampling interval of this study (2 m), and relatively small compared to
311 the entire observational depth (50 m). Therefore, we conclude that *B. infundibulum* did not perform
312 extensive DVM in our study region. The DVM of *Beroe* spp. has been reported for the northeast
313 Atlantic and the south Brazilian Bight (Roe et al., 1984; Júnior et al., 2015), but in the present study,
314 because of the low abundance, DVM could not be evaluated for *Beroe* sp. Several studies have

315 reported the DVM of scyphomedusae (Youngbluth and Båmstedt, 2001; Graham et al., 2001;
316 Gorbatenko et al., 2009; Brodeur et al., 2017). For *C. melanaster*, no DVM had been reported in
317 the southwestern Bering Sea shelf region (Brodeur et al., 2017), and in the present study, *C.*
318 *melanaster* was distributed above the pycnocline during both day and night.
319
320 *4.3. Horizontal and vertical distribution of ctenophores and scyphomedusae*
321 *4.3.1. Bolinopsis infundibulum*
322 The vertical distribution of *B. infundibulum* varied with the region and was distributed above the
323 pycnocline north of SLI, and below the pycnocline west of SLI. The region west of SLI was
324 characterized by an extremely cold water mass (<0°C) below the pycnocline (Fig. 3), and the
325 occurrence of *C. melanaster* above the pycnocline (Fig. 8). Therefore, the deep distribution of *B.*
326 *infundibulum* in the west of SLI could have been caused by both physical oceanographic factors and
327 biological interaction factors. We were unable assess the relative contributions of these variables.
328 A polynya was present in 2017 (Grebmeier, J.M. pers. comm.), and the loss of saline and
329 dense brine water during the formation of ice may have forced *B. infundibulum* to be distributed
330 below the pycnocline. Several ctenophores, *Mnemiopsis leidyi*, *Pleurobrachia* spp., and *Beroe*
331 spp., do not appear to cross a strong pycnocline, and instead distribute either above or below the
332 pycnocline (Roe et al., 1984; Vereshchaka, 2002; Haraldsson et al., 2014). When a strong

pycnocline developed west of SLI, *B. infundibulum* was restricted to below the pycnocline and did not appear to migrate upward across the pycnocline. *B. infundibulum* can live under cold (<0°C) conditions (Raskoff et al., 2005), and may be able to survive under the cold conditions that occur below the pycnocline in this region.

Due to predator-prey interactions, the occurrence of large scyphomedusae *C. melanaster* above the pycnocline west of SLI may have caused *B. infundibulum* to avoid that layer. GAM analysis revealed a negative interaction between these two species. *C. melanaster* feeds on gelatinous zooplankton (Purcell, 1991), and a prey-predator interaction between *C. melanaster* and *Bolinopsis* spp. has been noted off Japan (Kinoshita et al., 2006); thus, the distribution of *B. infundibulum* that we observed may have been a behavioural avoidance of predation by *C. melanaster*. Indeed, in the Nordic fjord, *B. infundibulum* has been shown to remain below the pycnocline to avoid predation from a large predatory scyphomedusae, *Cyanea capillata* (Båmstedt and Martinussen, 2015). However, in the Canada Basin, in the western Arctic Ocean, the coexistence of *C. melanaster* and *B. infundibulum* within the same depth layer has been reported (Raskoff et al., 2005; Purcell et al., 2010).

Although we identified two possible factors that may explain horizontal changes in the vertical distribution of *B. infundibulum*, physical oceanographic factors and biological interaction factors, we cannot conclude which factor is most important in determining the regional changes in

351 vertical distribution. *B. infundibulum* has been reported to occur at depths up to 1250 m in the
352 Oyashio Current in the western subarctic Pacific Ocean (Toyokawa et al., 2003) and Canada Basin,
353 in the western Arctic Ocean (Raskoff et al., 2005; Purcell et al., 2010). These findings suggest that
354 *B. infundibulum* exhibits much flexibility in terms of their vertical distribution and ability to adapt to
355 various environments and regions.
356
357 *4.3.2. Chrysaora melanaster* and *Beroe* sp.
358 We found that *C. melanaster* was distributed above the pycnocline at most stations, and the GAM
359 analysis revealed a significant positive interaction between *C. melanaster* abundance and
360 temperature ($p<0.01$, Table 1, Fig. 11). Previous studies have reported that *C. melanaster* is
361 distributed above the pycnocline (Brodeur, 1998; Brodeur et al., 2002; Raskoff et al., 2005;
362 Gorbatenko et al., 2009; Radchenko, 2013; Brodeur et al., 2017). Raskoff et al. (2005) reported
363 that the above pycnocline distribution of *C. melanaster* may be explained by their feeding on
364 copepods and gelatinous zooplankton, which are more abundant above the pycnocline. Radchenko
365 (2013) noted that the standing stock of zooplankton is more important than the thermal condition
366 above the pycnocline in explaining the vertical distribution of this species. Previous studies have
367 shown that *C. melanaster* feed on crustaceans, gelatinous zooplankton, larvae of walleye pollock,
368 ostracods, and decapod larvae in the Bering Sea (Brodeur et al., 2002; Zavolokin et al., 2008;

369 Ruzicka et al., 2020). Video images from the present study showed that hydromedusae *Aglantha*
370 *digitale* was abundant above the pycnocline (Maekakuchi unpublished data). Since *A. digitale* is
371 also an important food item for *C. melanaster* (Radchenko, 2013), we suggest that the observed
372 distribution of *C. melanaster* may be related to the abundance of their food items, such as copepods
373 and gelatinous zooplankton, above the pycnocline.
374 Standing stocks of *C. melanaster* were highest in the southern region in this study (south
375 of SLI). *C. melanaster* is very abundant in the southeastern Bering Sea shelf where it can exert a
376 substantial effect on other pelagic animals and marine food web structure in that region (Brodeur et
377 al., 2002, 2008), and *C. melanaster* has been reported in lower abundances farther north, in the
378 Canada Basin of the western Arctic Ocean (Raskoff et al., 2005; Purcell et al., 2010). These
379 observations suggest that the high standing stocks of *C. melanaster* in the southern region of this
380 study may reflect the regional differences in standing stocks.
381 The GAM analysis revealed a positive relationship between *Beroe* sp. and the abundance
382 of *B. infundibulum*. *Beroe* sp. were mainly distributed above the pycnocline, but they were
383 distributed below the pycnocline in the west of SLI, which parallels the regional pattern of vertical
384 distribution for *B. infundibulum* (Fig. 9). We suggest that predator-prey relationships may be the
385 cause of this parallel regional vertical distribution pattern of *Beroe* sp. with those of *B. infundibulum*.
386 *Beroe* spp. has been shown to feed on *B. infundibulum* (Greve, 1970; Purcell, 1991), and the vertical

387 distribution of *Beroe cucumis* has been documented to be similar to that of their prey (Falkenhaug,
388 1996; Bandara et al., 2016). However, as noted for *B. infundibulum*, *Beroe* sp. may be restricted in
389 their distribution to below the pycnocline due to highly saline water, so there could also be a
390 physical oceanographic mechanism affecting their distribution.
391
392 *4.4. Interannual changes in ctenophores and scyphomedusae*
393 This study was conducted in the same location and season over two consecutive years and standing
394 stocks of ctenophores and scyphomedusae were much lower in 2018 than in 2017, by a factor of
395 1/20 to 1/90. The biomass of large scyphomedusae in the southeastern Bering Sea has been shown
396 to fluctuate annually due to climate variability (Brodeur et al., 2017). There, the biomass of large
397 scyphomedusae, which is dominated by *C. melanaster*, increased 20-fold from 1975 to 2000, then
398 decreased to one-third of the maximum after 2001, possibly due to climate-induced changes in the
399 lower trophic levels (Brodeur et al., 2008). In warm years, ice melts quickly, leading to late
400 pycnocline development and phytoplankton bloom initiation; thus, smaller copepods such as
401 *Pseudocalanus* and *Acartia* dominate the zooplankton biomass (Hunt et al., 2011), which may result
402 in poor food conditions for *C. melanaster* (Brodeur et al., 2008). Conversely, in cold years, the
403 phytoplankton bloom initiates earlier, and large copepods, such as *Calanus,* dominate the
404 zooplankton biomass and these provide sufficient food conditions for the survival and growth of

405 ephyrae of *C. melanaster*, thus leading to an increase in scyphomedusae biomass (Brodeur et al.,
406 2008). Large changes in biomass over a short period have been observed in other regions. For
407 example, the biomass of ctenophores and scyphomedusae along the Kurile Islands in the Western
408 Pacific Ocean increased 10-fold from 2011 to 2012; intrusions from the Bering Sea and Okhotsk Sea
409 was invoked to explain this high biomass (Radchenko, 2013). Thus, there are large annual
410 fluctuations in the biomass of ctenophores and scyphomedusae, which are related to climate change
411 and oceanographic conditions.
412 Observations of water masses with high (>8°C) and low (<2°C) temperature conditions
413 that were characterized by a high abundance of *B. infundibulum* in 2017 were much more limited in
414 2018, and a decrease in optimal thermal conditions for *B. infundibulum* (>8 and <2°C) may explain
415 their very low abundance that year. Brodeur et al. (2017) reported that the biomass of *C.*
416 *melanaster* was high around SLI during both warm and cold periods. This suggests that around
417 SLI, conditions are suitable for the growth of *C. melanaster* polyps. Regarding annual differences
418 in the oceanographic conditions of this region between 2017 and 2018, the sea ice retreated in April
419 during 2018, which was approximately 1 month earlier than in 2017 (see Appendix F which is
420 derived from Arctic Data archive System (ADS) (https://ads.nipr.ac.jp/). As previously noted,
421 early ice retreat may induce late phytoplankton blooms, the dominance of small-sized copepods, and
422 low productivity, severely affecting food availability for *C. melanaster* (Brodeur et al., 2008). As

423 the sea ice began to retreat faster in 2018 compared with 2017, food conditions were likely to have
424 been poor for the survival and growth of the ephyrae of *C. melanaster*. The ephyrae of *C.*
425 *melanaster* grow in the spring to become medusae in summer and reach their peak level of biomass
426 in autumn (Zavolokin et al., 2008). Thus, the lower numbers of *C. melanaster* in 2018 may be
427 related to poor food conditions for their ephyra larvae, which in turn, may be related to the early ice
428 retreat that year.
429 The ctenophores, *B. infundibulum* and *Beroe* sp., which dominated in this region, spend
430 their entire life cycle in the plankton. Thus, annual differences in food conditions are experienced
431 during their early juvenile life-history phases. The main food for small ctenophores and ephyrae of
432 scyphomedusae is copepods (Purcell, 1991). Thus, the timing of the ice retreat underlies annual
433 differences in food conditions: early ice retreat leads to low productivity with a dominance of small
434 copepods, whilst late ice retreat leads to high productivity due to the dominance of large copepods
435 (Brodeur et al., 2008). For ctenophores and scyphomedusae in this region, low standing stocks in
436 2018 may be related to low productivity of large copepods, which was caused by the early ice retreat
437 in that year.
438
439 **Acknowledgments**
440 We thank the crew members of the T/S *Oshoro-Maru* and our collaborators, especially Toru

441 Hirawake, for assistance in collecting the video and CTD data. Constructive comments from
442 Richard D. Brodeur and one anonymous reviewer significantly improved the manuscript and are
443 highly appreciated. This work was conducted by the Arctic Challenge for Sustainability (ArCS)
444 Project (Program Grant Number JPMXD1300000000) and ArCS II. Part of this study was
445 supported by a Grant-in-Aid for Scientific Research 20H03054 (B), 19H03037(B), 18K14506 (Early
446 Career Scientists), and 17H01483 (A) from the Japan Society for the Promotion of Science (JSPS).

447 **References**

448 Båmstedt, U., Martinussen, M.B., 2015. Ecology and behavior of *Bolinopsis infundibulum*
449 (Ctenophora; Lobata) in the Northeast Atlantic. Hydrobiologia 759, 3–14.

450 Bandara, K., Varpe, Ø., Søreide, J., Wallenschus, J., Berge, J., Eiane, K., 2016. Seasonal vertical
451 strategies in a high-Arctic coastal zooplankton community. Mar. Ecol. Prog. Ser. 555, 49–
452 64.

453 Brodeur, R.D., 1998. In situ observations of the association between juvenile fishes and
454 scyphomedusae in the Bering Sea. Mar. Ecol. Prog. Ser. 163, 11–20.

455 Brodeur, R.D., Sugisaki, H., Hunt, G.L.Jr, 2002. Increases in jellyfish biomass in the Bering Sea:
456 implications for the ecosystem. Mar. Ecol. Prog. Ser. 233, 89–103.

457 Brodeur, R.D., Decker, M.B., Ciannelli, L., Purcell, J.E., Bond, N.A., Stabeno, P.J., Acuna, E., Hunt,
458 G.L.Jr, 2008. Rise and fall of jellyfish in the eastern Bering Sea in relation to climate regime
459 shifts. Prog. Oceanogr. 77, 103–111.

460 Brodeur, R., Cieciel, K., Zavolokin, A., 2017. Spatio-temporal variations of biomass and bloom.
461 conditions in regional seas. pp. 31–116, Uye, S.-I. and Brodeur, R.D. (eds), *Report of*
462 *Working Group 26 on Jellyfish Blooms around the North Pacific Rim: Causes and*
463 *Consequences.* PICES Sci. Rep. No. 51.

464 Comiso, J.C., Parkinson, C.L., Gersten, R., Stock, L., 2008. Accelerated decline in the Arctic sea ice
465 cover. Geophys. Res. Lett., 35, L01703, doi: 10.1029/2007GL031972.
466 Condon, R.H., Duarte, C.M., Pitt, K.A., Robinson, K.L., Lucas, C.H., Sutherland, K.R., Mianzan,
467 H.W., Bogeberg, M., Purcell, J.E., Decker, M.B., Uye, S., Madin, L.P., Brodeur, R.D.,
468 Haddock, S.H., Malej, A., Parry, G.D., Eriksen, E., Quiñones, J., Acha, M., Harvey, M.,
469 Arthur, J.M., Graham, W.M., 2013. Recurrent jellyfish blooms are a consequence of global
470 oscillations. Proc. Natl. Acad. Sci. 110, 1000–1005.
471 Cornwall, W., 2019. Vanishing Bering Sea ice poses climate puzzle. Science 364 (6441), 616–617.
472 Cowan, J.H.Jr, Houde, E.D., 1992. Size-dependent predation on marine fish larvae by ctenophores,
473 scyphomedusae, and planktivorous fish. Fish. Oceanogr. 1, 113–126.
474 Danielson, S., Eisner, L., Weingartner, T., Aagaard, K., 2011. Thermal and haline variability over
475 the central Bering Sea shelf: Seasonal and interannual perspectives. Cont. Shelf Res. 31,
476 539–554.
477 Danielson, S.L., Eisner, L., Ladd, C., Mordy, C., Sousa, L., Weingartner, T.J., 2017. A comparison
478 between late summer 2012 and 2013 water masses, macronutrients, and phytoplankton
479 standing crops in the northern Bering and Chukchi Seas. Deep-Sea Res. II 135, 7–26.
480 Duarte, C.M., Pitt, K.A., Lucas, C.H., Purcell, J.E., Uye, S.-I., Robinson, K., Brotz, L., Decker,
481 M.B., Sutherland, K.R., Malej, A., Madin, L., Mianzan, H., Gili, J.M., Fuentes, V., Atienza,

D., Pagés, F., Breitburg, D., Malek, J., Graham, W.M., Condon, R.H., 2013. Is global ocean sprawl a cause of jellyfish blooms? Front. Ecol. Environ. 11, 91–97.

Duffy-Anderson, J.T., Stabeno, P., Andrews, A.G.III, Cieciel, K., Deary, A., Farley, E., Fugate, C., Harpold, C., Heintz, R., Kimmel, D., Kuletz, K., Lamb, J., Paquin, M., Porter, S., Rogers, L., Spear, A., Yasumiishi, E., 2019. Responses of the northern Bering Sea and southeastern Bering Sea pelagic ecosystems following record-Breaking low winter sea ice. Geophys. Res. Lett. 46, 9833–9842.

Falkenhaug, T., 1996. Distribution and seasonal patterns of ctenophores in Malangen, northern Norway. Biol. Bull. 140, 59–70.

Gorbatenko, K.M., Nikolayev, A.V., Figurkin, A.L., Il'inskii, E.N., 2009. Quantitative composition, distribution, and feeding of large jellyfish (scyphozoa et hydrozoa) on the west Kamchatka shelf in summer. Russ. J. Mar. Biol. 35, 579–592.

Graham W.M., Pagès, F., Hamner, W.M., 2001. A physical context for gelatinous zooplankton aggregations: a review. Hydrobiologia 451, 199–212.

Graham, W.M., Martin, D.L., Martin, J.C., 2003. In situ observation and analysis of large jellyfish using a novel video profiler. Mar. Ecol. Prog. Ser. 254, 129–140.

Grebmeier, J.M., Cooper, L.W., 1995. Influence of the St. Lawrence Island polynya upon the Bering Sea benthos. J. Geophys. Res. 100 (C3), 4439–4460.

500 Greve, W., 1970. Cultivation experiments on North Sea ctenophores. Helgoländer wiss.
501 Meeresunters. 20, 304–317.
502 Han, C.-H., Uye, S.-I., 2009. Quantification of the abundance and distribution of the common
503 jellyfish *Aurelia aurita* s.l. with a Dual-frequency IDentification SONar (DIDSON). J.
504 Plankton Res. 31, 805–814.
505 Haraldsson, M., Båmstedt, U., Tiselius, P., Titelman, J., Aksnes, D.L., 2014. Evidence of diel
506 vertical migration in *Mnemiopsis leidyi*. PLoS ONE 9, e86595, doi:
507 10.1317/journal.pope.0086595.
508 Honda, N., Watanabe, T., 2007. Vertical distribution survey of the giant jellyfish *Nemopilema*
509 *nomurai* by an underwater video camera attached to a midwater trawl net. Nippon Suisan
510 Gakkaishi 73, 1042–1048.
511 Honda, N., Toyokawa, M., Shimizu, M., Fujii, N., Fujita, K., 2016. Research methods for
512 distribution and size measuring of large jellyfishes (*Nemopilema nomurai, Rhopilema*
513 *esculentum* and *Aurelia aurita* s.l.) by using acoustic camera. Fish. Engineer. 53, 87–96.
514 Hunt, G.L., Coyle, K.O., Eisner, L.B., Farley, E.V., Heintz, R.A., Mueter, F., Napp, J.M., Overland,
515 J.E., Ressler, P.H., Salo, S., Stabeno, P.J., 2011. Climate impacts on eastern Bering Sea
516 foodwebs: a synthesis of new data and an assessment of the Oscillating Control Hypothesis.
517 ICES J. Mar. Sci. 68 (6), 1230–1243.

518 Huntington, H.P., Danielson, S.L., Wiese, F.K., Baker, M., Boveng, P., Citta, J., De Robertis, A.,
519 Dickson, D., Farley, E., George, J.C., Iken, K., Kimmel, D., Kuletz, K., Ladd, C., Levine,
520 R., Quakenbush, L., Stabeno, P.J., Stafford, K.M., Stockwell, D., Wilson, C., 2020.
521 Evidence suggests potential transformation of the Pacific Arctic ecosystem is underway.
522 Nat. Clim. Chang. 10, 342–348.
523 Júnior, M.N., Brandini, F.P., Codina, J.C.U., 2015. Diel vertical dynamics of gelatinous zooplankton
524 (cnidaria, ctenophora and thaliacea) in a subtropical stratified ecosystem (south Brazilian
525 bight). PLoS ONE 10, e0144161, doi: 10.1371/ journal.pone.0144161.
526 Kawamura, A., 1989. Fast sinking mouth ring for closing Norpac net. Nippon Suisan Gakkaishi 55,
527 1121.
528 Kinoshita, J., Hiromi, J., Yamada, Y., 2006. Abundance and biomass of scyphomedusae, *Aurelia*
529 *aurita* and *Chrysaora melanaster*, and ctenophora, *Bolinopsis mikado*, with estimates of
530 their feeding impact on zooplankton in Tokyo Bay, Japan. J. Oceanogr. 62, 607–615.
531 Nogata, Y., Endo, N., Ishii, H., Matsumura, K., Sakaguchi, I., 2009. Underwater video camera
532 system for monitoring vertical distribution of jellyfish *Aurelia aurita*. CRIEPI Res. Rep.
533 8050, 1–10.
534 Parkinson, C.L., Comiso, J.C., 2013. On the 2012 record low Arctic sea ice cover: Combined impact
535 of preconditioning and an August storm. Geophys. Res. Lett. 40, 1356–1361.

536 Pennak, R.W., 1943. An effective method of diagramming diurnal of zooplankton organisms.
537 Ecology 24, 405–407.
538 Purcell, J.E., 1991. A review of cnidarians and ctenophores feeding on competitors in the plankton.
539 Hydrobiologia 216, 335–342.
540 Purcell, J.E., Brown, E.D., Stokesbury, K.D.E., Haldorson, L.H., Shirley, T.C., 2000. Aggregations
541 of the jellyfish *Aurelia labiata*: abundance, distribution, association with age-0 walleye
542 pollock, and behaviors promoting aggregation in Prince William Sound, Alaska, USA. Mar.
543 Ecol. Prog. Ser. 195, 145–158.
544 Purcell, J.E., Uye, S.-I., Lo, W.T., 2007. Anthropogenic causes of jellyfish blooms and their direct
545 consequences for humans: a review. Mar. Ecol. Prog Ser. 350, 153–174.
546 Purcell, J.E., Hopcroft, R.R., Kosobokova, K.N., Whitledge, T.E., 2010. Distribution, abundance,
547 and predation effects of epipelagic ctenophores and jellyfish in the western Arctic Ocean.
548 Deep-Sea Res. II 57, 127–135.
549 Radchenko, K.V., 2013. New data on distribution and feeding habits of jellyfish in the northwest
550 Pacific. Russ. J. Mar. Biol. 39, 509–520.
551 Raskoff, K.A., Purcell, J.E., Hopcroft, R.R., 2005. Gelatinous zooplankton of the Arctic Ocean: in
552 situ observations under the ice. Polar Biol. 28, 207–217.

553 Raskoff, K.A., Hopcroft, R.R., Purcell, J.E., Youngbluth, M., 2010. Jellies under ice: ROV
554 observations from the Arctic 2005 hidden ocean expedition. Deep-Sea Res. II 57, 111–126.
555 Robinson, K.L., Ruzicka, J.J., Decker, M.B., Brodeur, R.D., Hernandez, F.J., Quiñones, J., Acha, E.
556 M., Uye, S.-I., Mianzan, H. and Graham W.M., 2014. Jellyfish, forage fish, and the world's
557 major fisheries. Oceanogr. 27, 104–115.
558 Roe, H.S.J., James, P.T., Thurston, M.H., 1984. The diel migrations and distribution with in a
559 mesopelagic community in the North East Atlantic. 6. medusae, ctenophores, amphipods
560 and euphausiids. Prog. Oceanogr. 13, 425–460.
561 Ruzicka, J., Brodeur, R.D., Cieciel, K., Decker, M.B., 2020. Examining the ecological role of
562 jellyfish in the Eastern Bering Sea. ICES J. Mar. Sci. 77, 791–802.
563 Sasaki, H., Matsuno, K., Fujiwara, A., Onuka, M., Yamaguchi, A., Ueno, H., Watanuki, Y., Kikuchi
564 T., 2016. Distribution of Arctic and Pacific copepods and their habitat in the northern
565 Bering and Chukchi seas. Biogeosciences 13, 4555–4567.
566 Shimada, K., Kamoshida, T., Itoh, M., Nishino, S., Carmack, E., McLaughlin, F., Zimmermann, F.,
567 Proshutinsky, A., 2006. Pacific Ocean inflow: Influence on catastrophic reduction of sea ice
568 cover in the Arctic Ocean. Geophys. Res. Lett. 33, L08605, doi: 10.1029/2005GL025624.
569 Sokal, R.R., Rohlf, F.J., 1995. Biometry: The Principles and Practice of Statistics in Biological
570 Research. 3rd Ed., W.H. Freeman and Co., New York.

571 Stabeno, P.J., Bell, S.W., 2019. Extreme conditions in the Bering Sea (2017–2018): Record-breaking
572 low sea-ice extent. Geophys. Res. Lett. 46, 8952–8959.
573 Toyokawa, M., Toda, T., Kikuchi, T., Miyake, H., Hashimoto, J., 2003. Direct observations of a
574 dense occurrence of *Bolinopsis infundibulum* (Ctenophora) near the seafloor under the
575 Oyashio and notes on their feeding behavior. Deep-Sea Res. I 50, 809–813.
576 Uye, S.-I., Brodeur, R., Ishii, H., Zavolokin, A., 2017. Sampling considerations. pp. 21–29, Uye, S.-
577 I. and Brodeur, R.D. (eds), Report of Working Group 26 on Jellyfish Blooms around the
578 North Pacific Rim: Causes and Consequences. PICES Sci. Rep. No. 51.
579 Vereshchaka, A.L., 2002. Small-scale vertical and behavior of the ctenophore *Beroe* in the Black
580 Sea off Gelendzhik. Mar. Biol. 42, 811–814.
581 Wood, S.N., 2017. Generalized Additive Models: An Introduction with R 2nd Ed., CRC Press, Boca
582 Raton.
583 Youngbluth, M.J., Båmstedt, U., 2001. Distribution, abundance, behavior and metabolism of
584 *Periphylla periphylla*, a mesopelagic coronate medusa in a Norwegian fjord. Hydrobiologia
585 451, 321–333.
586 Zavolokin, A.V., Glebov, I.I., Kosenok, N.S., 2008. Distribution, quantitative composition, and
587 feeding of Jellyfish in the western Bering Sea in summer and fall. Russ. J. Mar. Biol. 34,
588 461–467.

590 **Table and figure captions**

591 Table 1. Results of generalized additive models (GAM) based on the abundance of ctenophores
592 and scyphomedusae (*Bolinopsis infundibulum, Chrysaora melanaster, Beroe* sp.), and
593 environmental parameters: depth, temperature, salinity, the effect of pycnocline (U: upper),
594 day/night, and species interactions of other jellyfishes. +: positive, -: negative, *: $p < 0.05$,
595 **: $p < 0.01$, ***: $p < 0.001$. Detailed patterns between each parameter are presented in
596 Fig. 11.

597 Fig. 1. Location of the stations used to observe ctenophores and scyphomedusae by frame camera
598 in the northern Bering Sea in 9–22 July 2017 (left) and 2–12 July 2018 (right). Numbers in
599 italics denote the depth strata in meters.

600 Fig. 2. Captured images (A): *Bolinopsis infundibulum* (a), *Chrysaora melanaster* (b), *Beroe* sp. (c).
601 Frame camera (B): video camera (a), current fin (b), weight (20 kg x 4) (c), observation
602 frame (d), halogen light (x 2) (e), electronic data cable (f). Schema shows the calculation
603 of the observed volume (C). For details, see the text.

604 Fig. 3. Temperature (upper) and salinity (lower) cross-sections at each line set in the northern Bering
605 Sea during 9–22 July 2017. The location of each line is shown in the upper-right map.

606 Fig. 4. Temperature (upper) and salinity (lower) cross-sections at each line set in the northern
607 Bering Sea during 2–12 July 2018. The location of each line is shown in the upper-right
608 map.
609 Fig. 5. Horizontal distribution of standing stock (ind. $m^{-2}$) of *Bolinopsis infundibulum* (left),
610 *Chrysaora melanaster* (middle), and *Beroe* sp. (right) in the northern Bering Sea during 9–
611 22 July 2017 (upper) and 2–12 July 2018 (lower).
612 Fig. 6. Diel changes in the vertical distribution of *Bolinopsis infundibulum* at four stations (St. 10,
613 14, 20, 23) in the northern Bering Sea during 9–22 July 2017. Thick bars represent the
614 distribution core ($D_{25\%}$–$D_{75\%}$) split with the distribution centre ($D_{50\%}$). Thin bars show the
615 ranges of $D_{10\%}$ and $D_{90\%}$. Horizontal black bars at the top indicate night-time samplings.
616 Shaded zones represent the sea bottom. Triangles represent pycnocline depths. Details of
617 each observation are presented in Appendix C (St. 10) and Appendix D (Sts. 14, 20, 23).
618 Fig. 7. Vertical distribution of temperature, salinity, and *Bolinopsis infundibulum* in the northern
619 Bering Sea during 9–22 July 2017. Triangles represent pycnocline depths.
620 Fig. 8. Vertical distribution of temperature, salinity and *Chrysaora melanaster* in the northern
621 Bering Sea during 9–22 July 2017. Triangles represent pycnocline depths.
622 Fig. 9. Vertical distribution of temperature, salinity and *Beroe* sp. in the northern Bering Sea
623 during 9–22 July 2017. Triangles represent pycnocline depths.

624 Fig. 10. T-S diagrams of all stations in 2017 (left) and 2018 (right) (A). Abundance (ind. $m^{-3}$) of
625 *Bolinopsis infundibulum* at 2 m intervals is shown by bubble plots on T-S diagrams (B).
626 Fig. 11. Result of the generalized additive model (GAM) based on abundance anomalies of three
627 large gelatinous zooplankton with environmental parameters.
628 Appendix A (Table). Data for ctenophores and scyphomedusae observations in the northern Bering
629 Sea during 9–22 July 2017 and 2–12 July 2018. One cast required approximately 20 min.
630 To evaluate day-night differences, 11 observations were made at 1 h intervals at St. 10 from
631 19:40 13 July to 7:10 14 July 2017. During that period, seven day (19:40, 21:15, 23:12,
632 0:15, 6:10, 7:10) and four night (1:12, 2:13, 3:12, 4:13) casts were made. Observed
633 volume ($m^3$) and total counts of each species are also shown for each cast.
634 Appendix B (Figure). Scatter plot on the density of *Bolinopsis infundibulum* quantified during
635 descent and ascent.
636 Appendix C (Figure). Diel changes in the vertical distribution of *Bolinopsis infundibulum* at St. 10
637 during 13–14 July 2017. Open and solid markers represent day and night, respectively.
638 Appendix D (Figure). Day (open) and night (solid) vertical distribution of *Bolinopsis infundibulum*
639 at St. 14, 20, 23 during 17–21 July 2017.
640 Appendix E (Figure). Contour plots for abundance anomalies of three large gelatinous zooplankton
641 on a T-S diagram.

642 Appendix F (Figure). Sea ice concentration on April 1st in 2017 (left) and 2018 (right). Images
643 were downloaded from the Arctic Data archive System (ADS) (https://ads.nipr.ac.jp/).
644 Video supplemental material 1: Example of video image captured at St. 10 (cast 14) on 14 July
645 2017.
646 Video supplemental material 2: Example of video image captured at St. 19 (cast 27) on 19 July
647 2017.

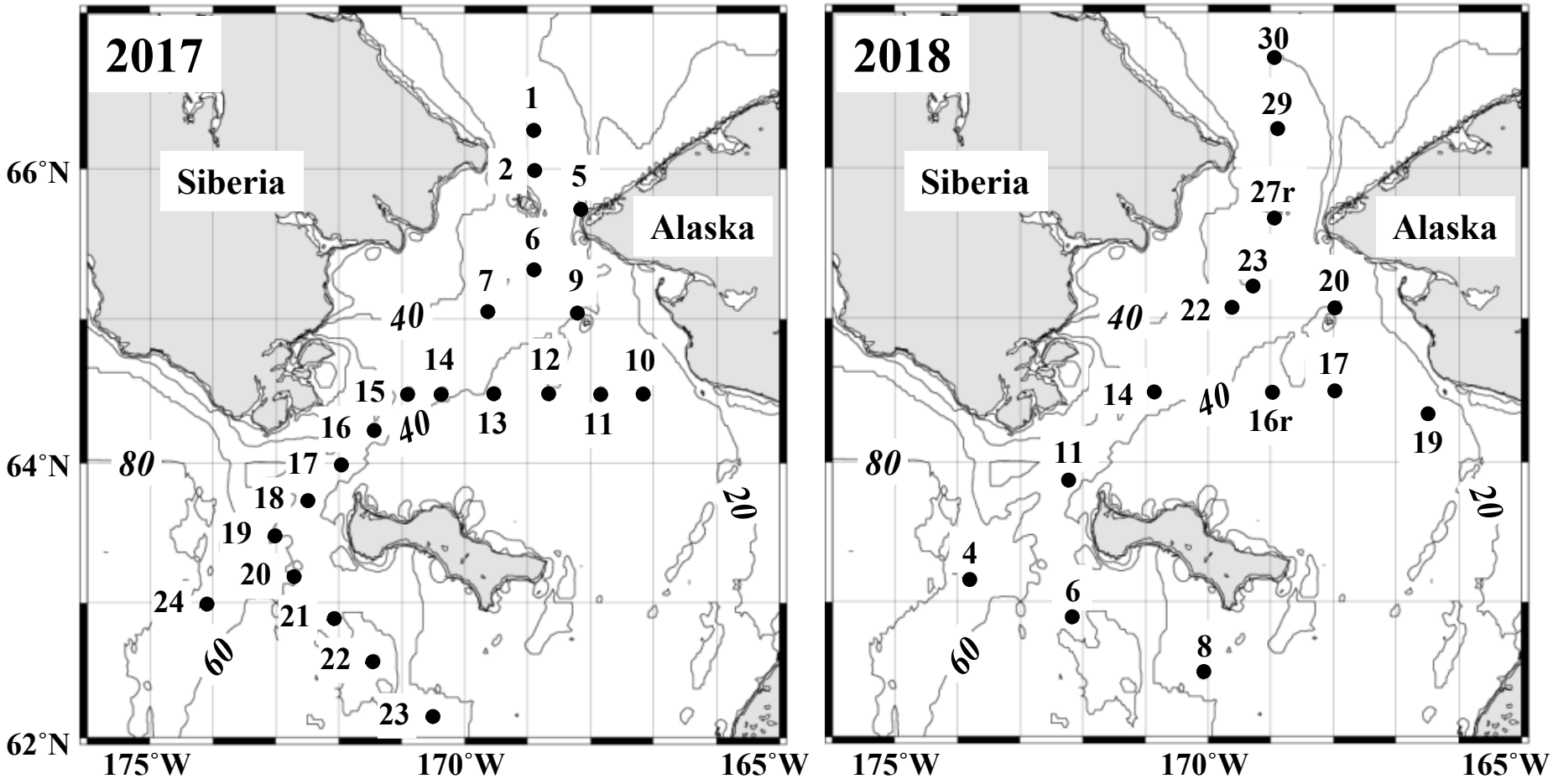


Fig. 1. Location of the stations used to observe ctenophores and scyphomedusae by frame camera in the northern Bering Sea in 9–22 July 2017 (left) and 2–12 July 2018 (right). Numbers in italics denote the depth strata in meters.

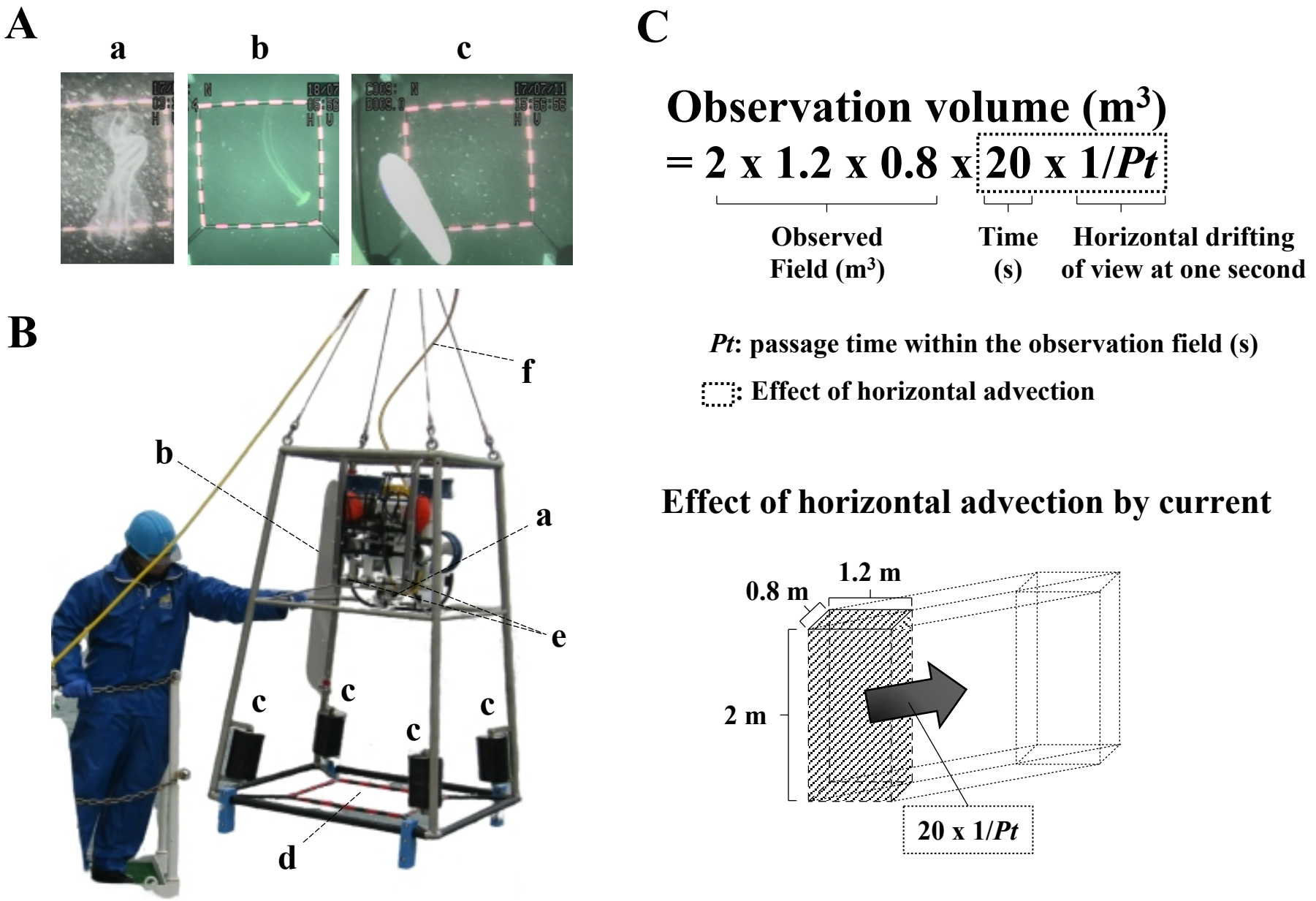


Fig. 2. Captured images (A): *Bolinopsis infundibulum* (a), *Chrysaora melanaster* (b), *Beroe* sp. (c). Frame camera (B): video camera (a), current fin (b), weight (20 kg x 4) (c), observation frame (d), halogen light (x 2) (e ), electronic data cable (f). Schema shows the calculation of the observed volume (C). For details, see the text.

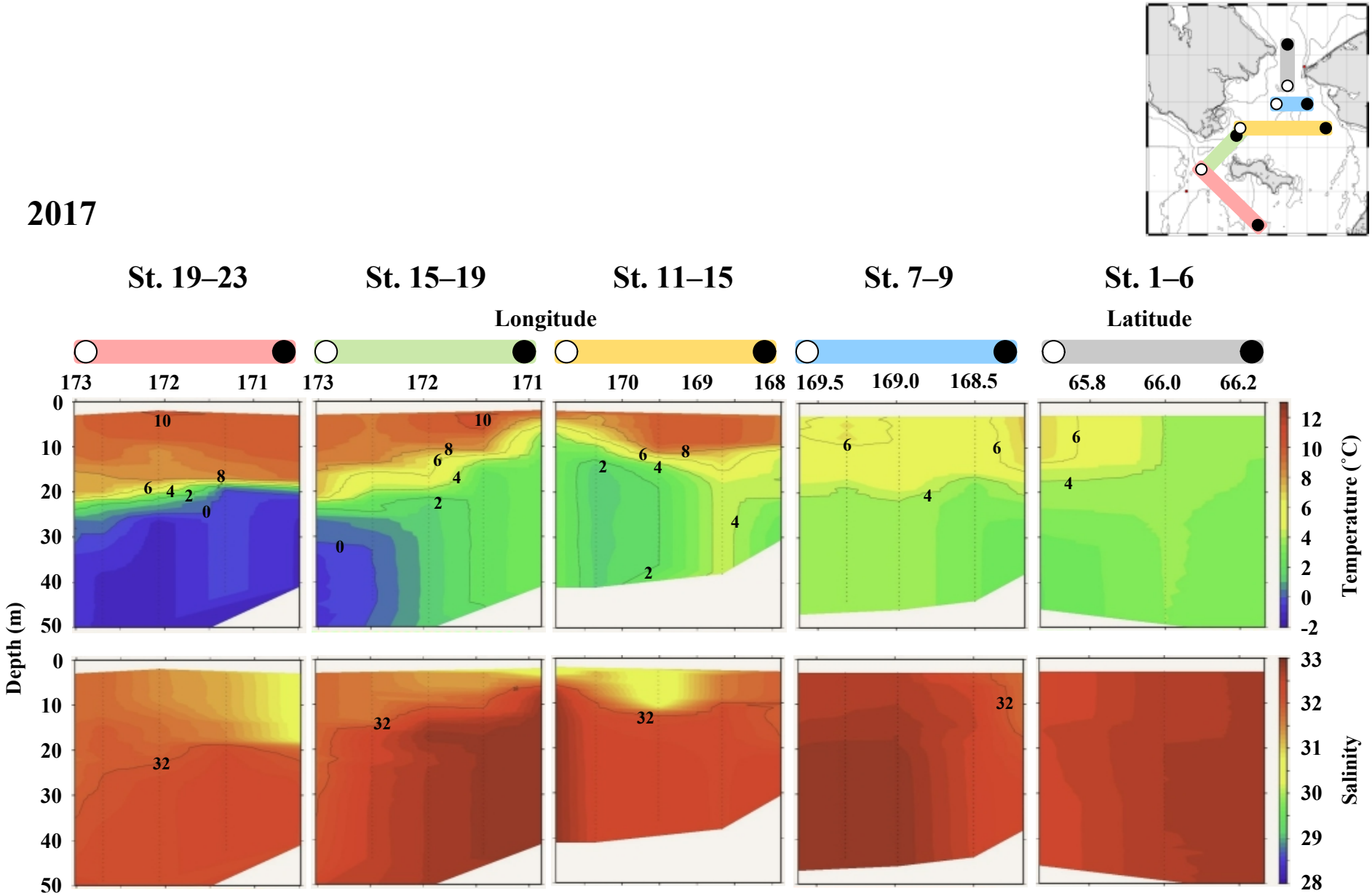


Fig. 3. Temperature (upper) and salinity (lower) cross-sections at each line set in the northern Bering Sea during 9–22 July 2017. The location of each line is shown in the upper-right map.

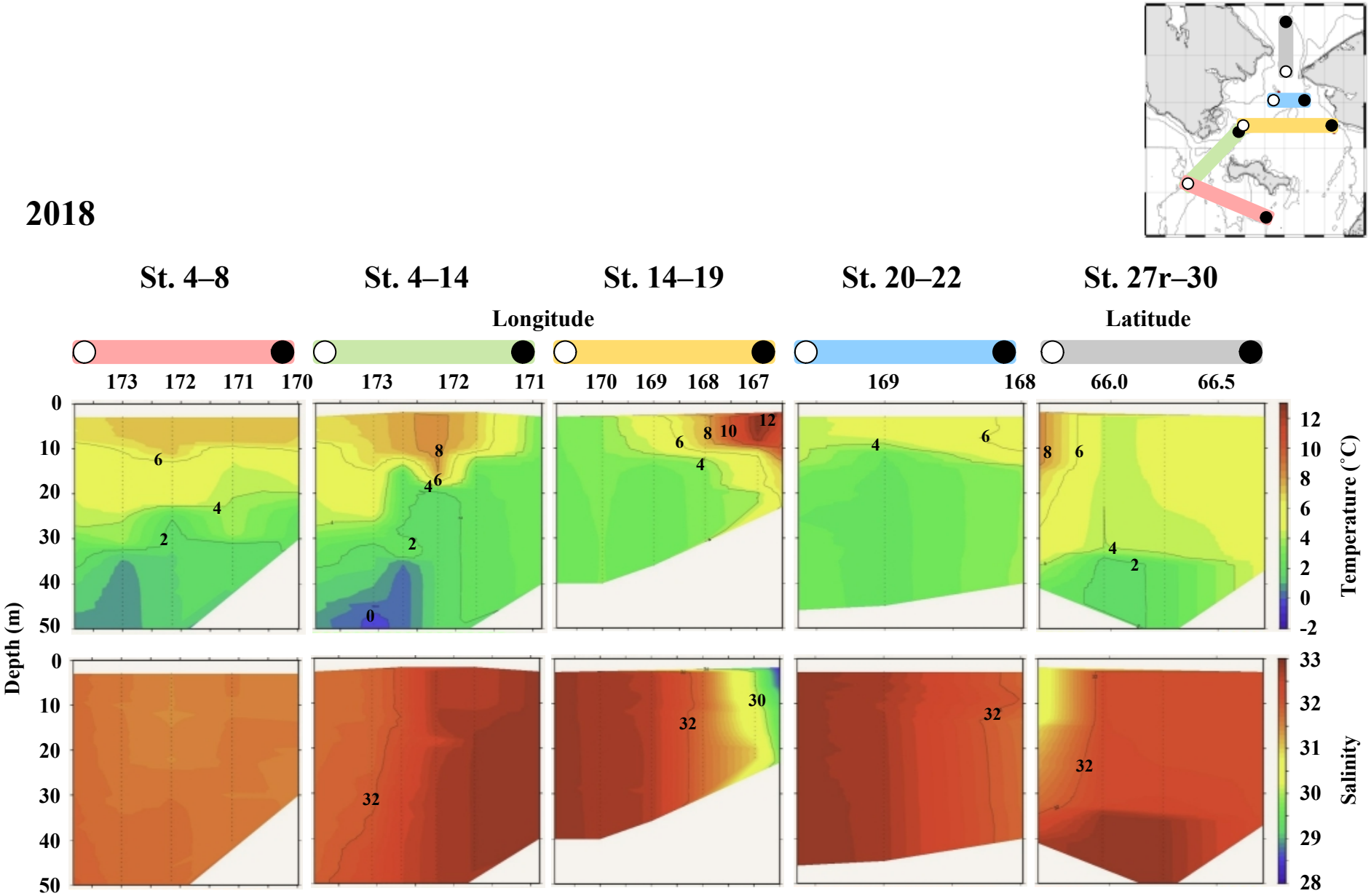


Fig. 4. Temperature (upper) and salinity (lower) cross-sections at each line set in the northern Bering Sea during 2–12 July 2018. The location of each line is shown in the upper-right map.

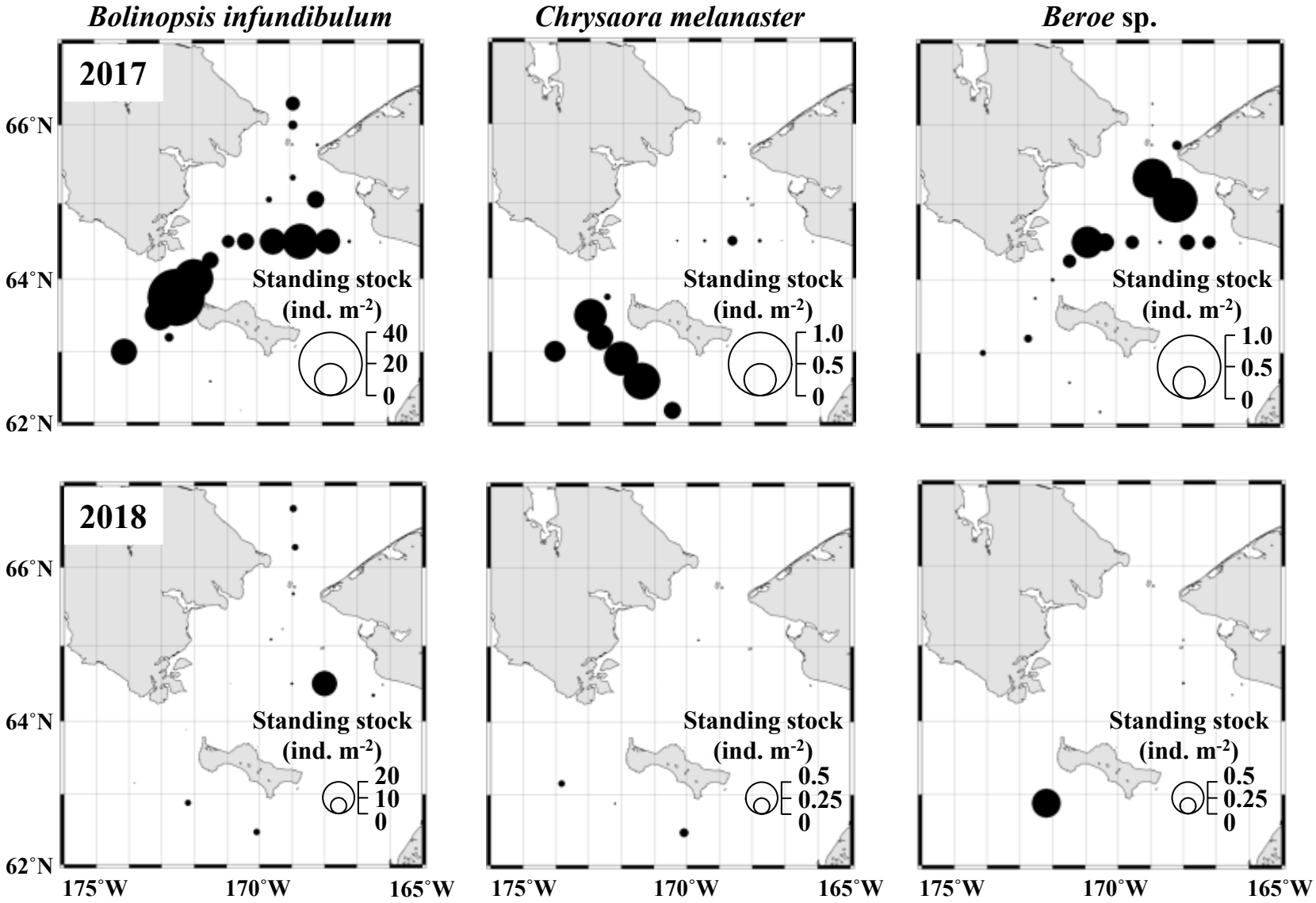


Fig. 5. Horizontal distribution of standing stock (ind. $m^{-2}$) of *Bolinopsis infundibulum* (left), *Chrysaora melanaster* (middle), and *Beroe* sp. (right) in the northern Bering Sea during 9–22 July 2017 (upper) and 2–12 July 2018 (lower).

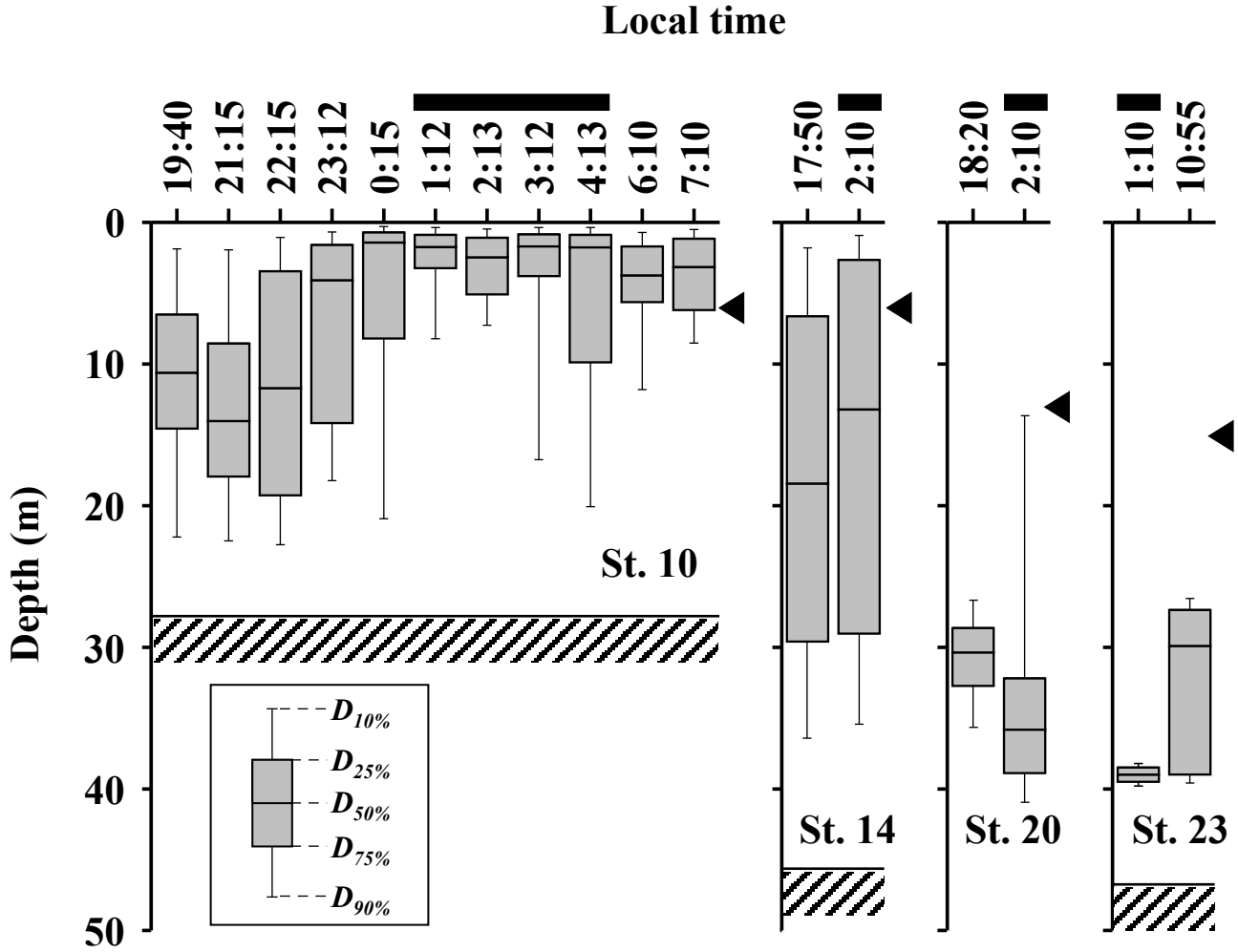


Fig. 6. Diel changes in the vertical distribution of *Bolinopsis infundibulum* at four stations (St. 10, 14, 20, 23) in the northern Bering Sea during 9–22 July 2017. Thick bars represent the distribution core ($D_{25\%} - D_{75\%}$) split with the distribution centre ($D_{50\%}$). Thin bars show the ranges of $D_{10\%}$ and $D_{90\%}$. Horizontal black bars at the top indicate night-time samplings. Triangles represent pycnocline depths. Details of each observation are presented in Electronic Supplement 1 (St. 10) and 2 (Sts. 14, 20, 23).

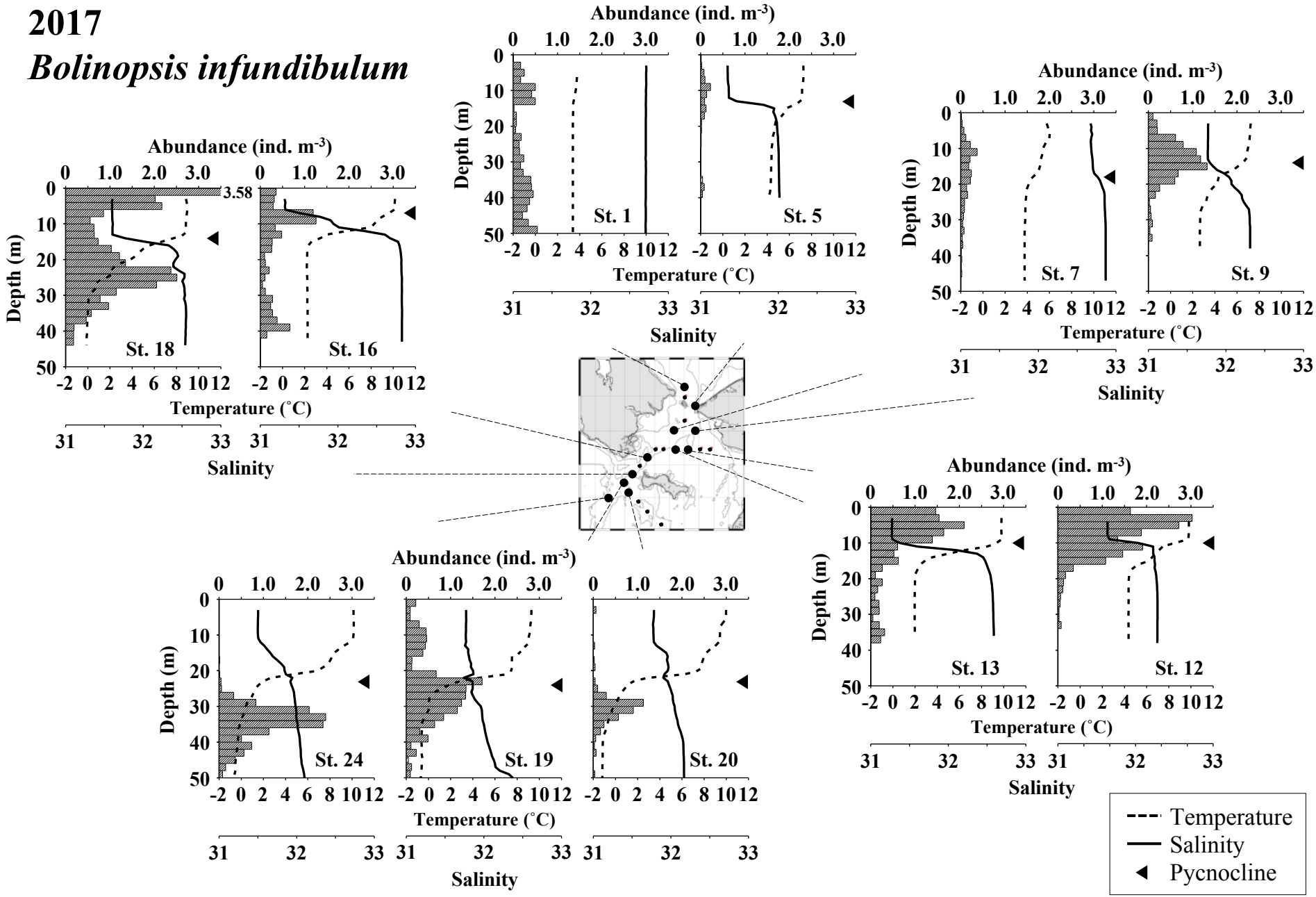


Fig. 7. Vertical distribution of temperature, salinity, and *Bolinopsis infundibulum* in the northern Bering Sea during 9–22 July 2017. Triangles represent pycnocline depths.

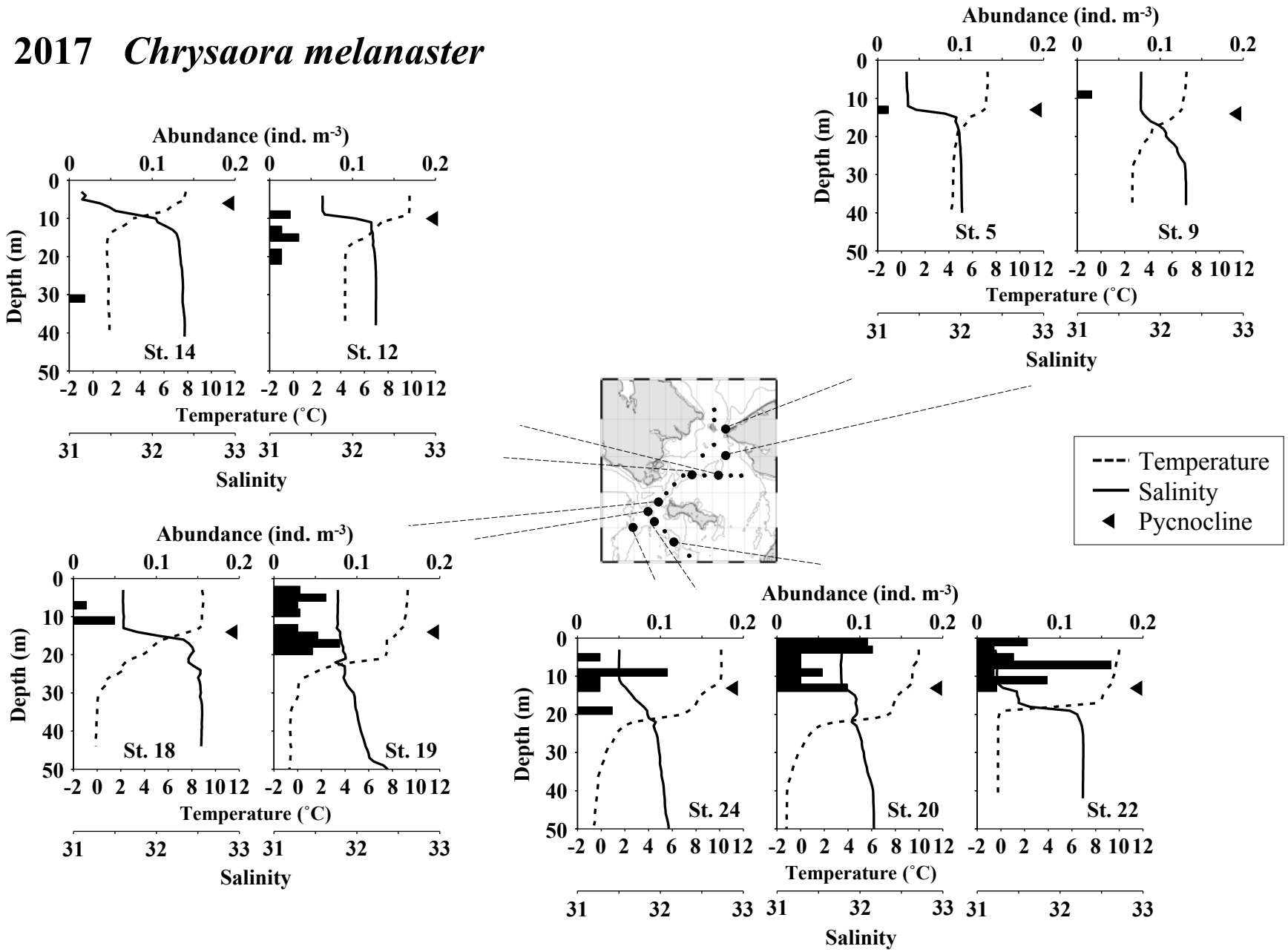


Fig. 8. Vertical distribution of temperature, salinity and *Chrysaora melanaster* in the northern Bering Sea during 9–22 July 2017. Triangles represent pycnocline depths.

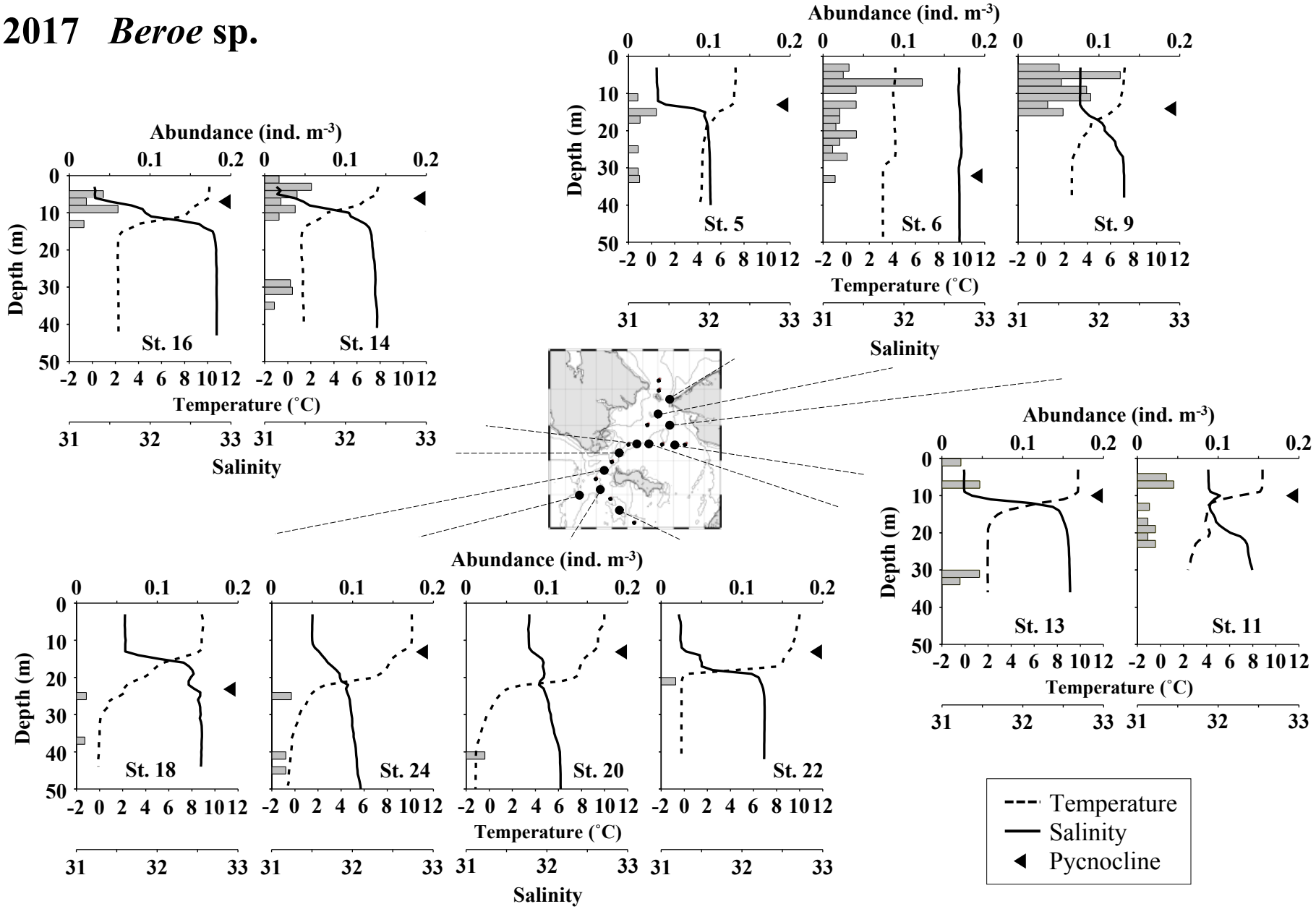


Fig. 9. Vertical distribution of temperature, salinity and *Beroe* sp. in the northern Bering Sea during 9–22 July 2017. Triangles represent pycnocline depths.

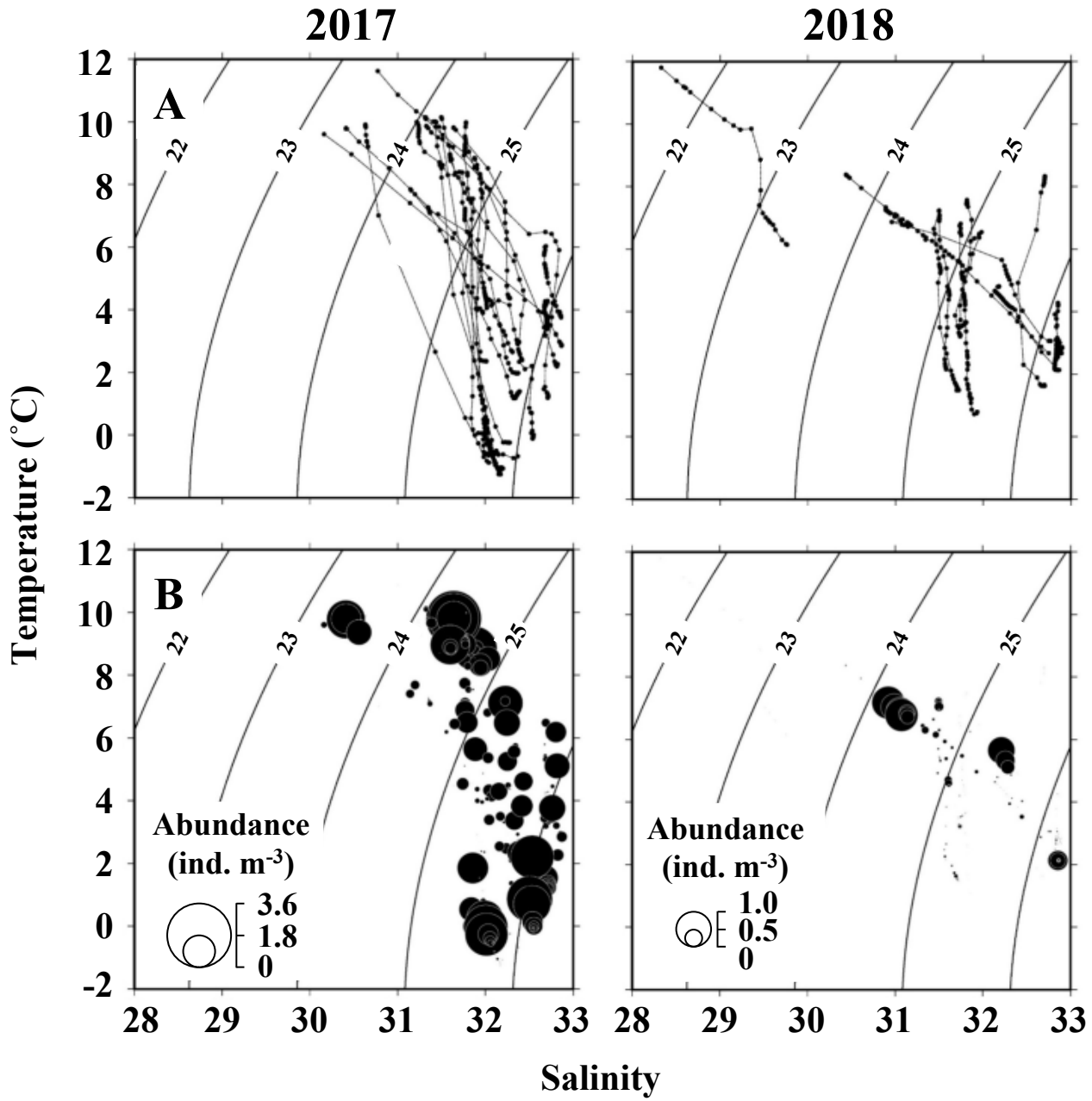


Fig. 10. T-S diagrams of all stations in 2017 (left) and 2018 (right) (A). Abundance (ind. $m^{-3}$) of *Bolinopsis infundibulum* at 2 m intervals is shown by bubble plots on T-S diagrams (B).

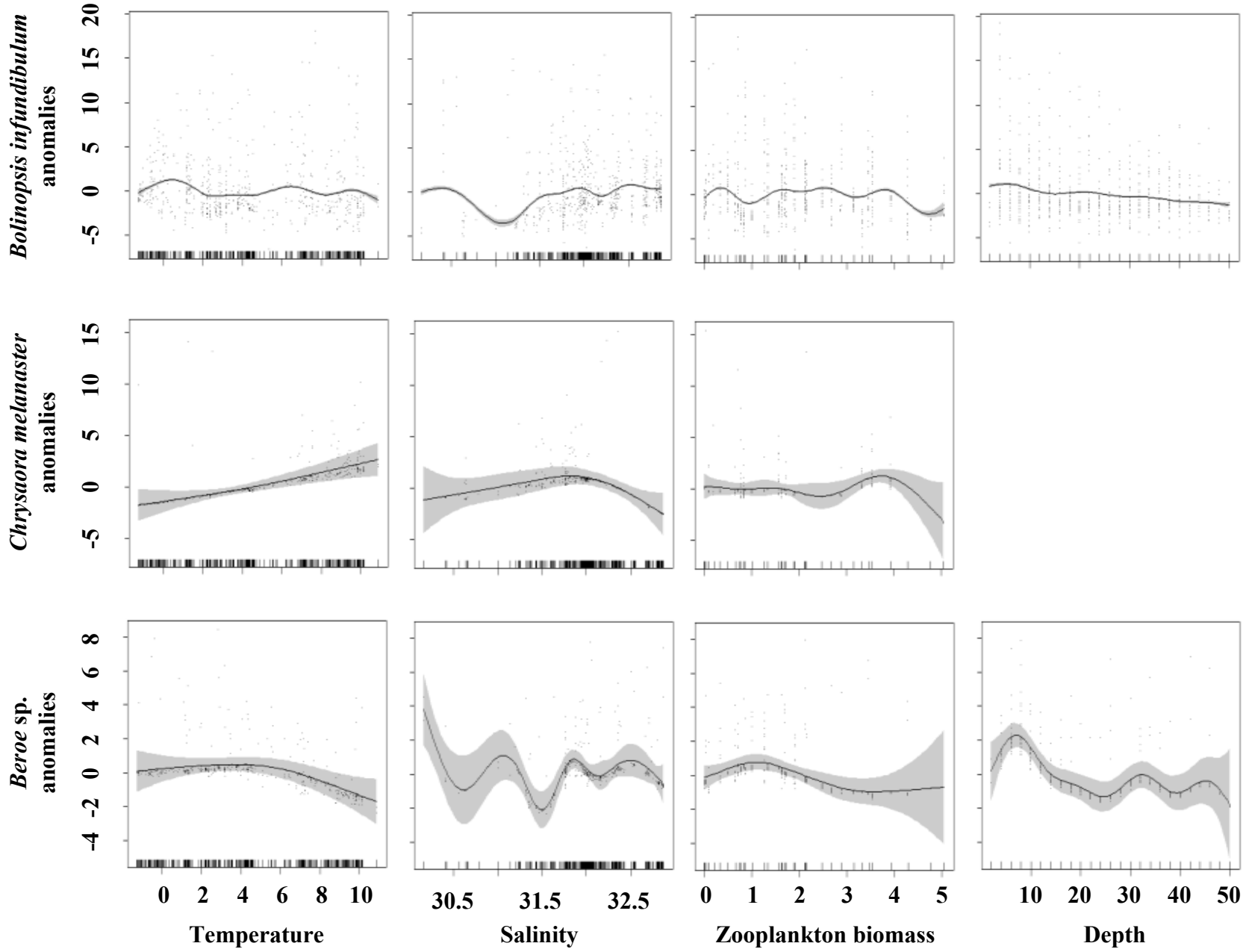


Fig. 11. Result of generalized additive model (GAM) based on abundance anomalies of three large gelatinous zooplankton with environmental parameters.

Appendix A. Data for ctenophores and scyphomedusae observations in the northern Bering Sea during 9–22 July 2017 and 2–12 July 2018. One cast required approximately 20 min. To evaluate day-night differences, 11 observations were made at 1 h intervals at St. 10 from 19:40 13 July to 7:10 14 July 2017. During that period, seven day (19:40, 21:15, 23:12, 0:15, 6:10, 7:10) and four night (1:12, 2:13, 3:12, 4:13) casts were made. Observed volume ($m^3$) and total counts of each species during descent and ascent of each cast are also shown.

| Year | Station | | Position | | Local time | | Day/night | Descent | | | | Ascent | | | |
|---|---|---|---|---|---|---|---|---|---|---|---|---|---|---|---|
| | | | | | | | | Observed | Number of counted | | | Observed | Number of counted | | |
| | (depth m) | Cast | Lat. (N) | Lon. (W) | Date | Hour | | volume ($m^3$) | *B. infundibulum* | *C. melanaster* | *Beroe* sp. | volume ($m^3$) | *B. infundibulum* | *C. melanaster* | *Beroe* sp. |
| 2017 | | | | | | | | | | | | | | | |
| | 1 (57) | 1 | 66˚16’ | 168˚54’ | 9 July | 13:00 | Day | 677.8 | 221 | 0 | 1 | 688.9 | 111 | 0 | 0 |
| | 2 (53) | 2 | 66˚00’ | 168˚54’ | 10 July | 3:40 | Night | 1105.4 | 215 | 0 | 0 | 1069.1 | 177 | 0 | 1 |
| | 5 (44) | 3 | 65˚45’ | 168˚09’ | 11 July | 9:00 | Day | 701.9 | 59 | 1 | 2 | 818.1 | 17 | 0 | 5 |
| | 6 (55) | 4 | 65˚20’ | 168˚54’ | 11 July | 16:30 | Day | 780.5 | 77 | 0 | 10 | 946.0 | 113 | 1 | 13 |
| | 7 (51) | 5 | 65˚03’ | 169˚38’ | 12 July | 8:45 | Day | 995.0 | 89 | 0 | 0 | 934.6 | 100 | 0 | 0 |
| | 9 (42) | 6 | 65˚03’ | 168˚12’ | 13 July | 10:00 | Day | 697.8 | 262 | 1 | 20 | 620.8 | 163 | 0 | 8 |
| | 10 (28) | 7 | 64˚30’ | 167˚10’ | 13 July | 19:40 | Day | 496.0 | 48 | 0 | 2 | 492.6 | 15 | 0 | 3 |
| | 10 (28) | 8 | 64˚30’ | 167˚10’ | 13 July | 21:15 | Day | 547.2 | 35 | 0 | 9 | 475.4 | 15 | 0 | 7 |
| | 10 (28) | 9 | 64˚30’ | 167˚10’ | 13 July | 22:15 | Day | 428.4 | 16 | 0 | 1 | 340.7 | 14 | 0 | 5 |
| | 10 (28) | 10 | 64˚30’ | 167˚10’ | 13 July | 23:12 | Day | 478.2 | 20 | 0 | 9 | 274.3 | 3 | 0 | 3 |
| | 10 (28) | 11 | 64˚30’ | 167˚10’ | 14 July | 0:15 | Day | 508.4 | 25 | 0 | 5 | 438.0 | 58 | 0 | 2 |
| | 10 (28) | 12 | 64˚30’ | 167˚10’ | 14 July | 1:12 | Night | 459.5 | 30 | 0 | 0 | 297.4 | 35 | 0 | 5 |
| | 10 (28) | 13 | 64˚30’ | 167˚10’ | 14 July | 2:13 | Night | 452.6 | 62 | 0 | 5 | 272.0 | 73 | 0 | 2 |
| | 10 (28) | 14 | 64˚30’ | 167˚10’ | 14 July | 3:12 | Night | 342.6 | 93 | 0 | 7 | 297.1 | 44 | 1 | 7 |
| | 10 (28) | 15 | 64˚30’ | 167˚10’ | 14 July | 4:13 | Night | 430.4 | 18 | 0 | 3 | 357.0 | 27 | 0 | 6 |
| | 10 (28) | 16 | 64˚30’ | 167˚10’ | 14 July | 6:10 | Day | 282.9 | 32 | 0 | 5 | 250.6 | 15 | 0 | 4 |
| | 10 (28) | 17 | 64˚30’ | 167˚10’ | 14 July | 7:10 | Day | 285.3 | 43 | 0 | 3 | 305.9 | 18 | 0 | 2 |
| | 11 (34) | 18 | 64˚30’ | 167˚50’ | 16 July | 20:12 | Day | 615.9 | 400 | 1 | 6 | 504.9 | 300 | 1 | 4 |
| | 12 (42) | 19 | 64˚30’ | 168˚40’ | 17 July | 3:50 | Night | 710.2 | 549 | 3 | 2 | 475.3 | 320 | 2 | 0 |
| | 13 (40) | 20 | 64˚30’ | 169˚31’ | 17 July | 11:40 | Day | 425.4 | 161 | 0 | 5 | 361.3 | 271 | 1 | 1 |
| | 14 (46) | 21 | 64˚30’ | 170˚21’ | 17 July | 17:50 | Day | 609.2 | 227 | 1 | 5 | 651.0 | 279 | 0 | 10 |
| | 14 (46) | 22 | 64˚30’ | 170˚21’ | 18 July | 2:10 | Night | 724.2 | 146 | 0 | 4 | 815.5 | 304 | 1 | 5 |
| | 15 (45) | 23 | 64˚30’ | 170˚53’ | 18 July | 10:50 | Day | 677.3 | 187 | 0 | 17 | 521.8 | 116 | 0 | 4 |
| | 16 (47) | 24 | 64˚15’ | 171˚26’ | 18 July | 16:40 | Day | 680.5 | 206 | 0 | 2 | 569.9 | 197 | 0 | 5 |
| | 17 (53) | 25 | 64˚00’ | 171˚57’ | 18 July | 21:50 | Day | 935.0 | 783 | 0 | 0 | 889.6 | 487 | 0 | 2 |
| | 18 (48) | 26 | 63˚45’ | 172˚29’ | 19 July | 3:50 | Night | 870.1 | 1026 | 1 | 2 | 880.8 | 861 | 3 | 0 |
| | 19 (65) | 27 | 63˚30’ | 173˚00’ | 19 July | 10:55 | Day | 661.7 | 324 | 6 | 0 | 522.8 | 283 | 7 | 0 |
| | 20 (66) | 28 | 63˚12’ | 172˚42’ | 19 July | 18:20 | Day | 658.7 | 79 | 7 | 0 | 561.1 | 109 | 9 | 1 |
| | 20 (66) | 29 | 63˚12’ | 172˚42’ | 20 July | 2:10 | Night | 731.5 | 69 | 3 | 4 | 678.7 | 130 | 3 | 4 |
| | 21 (54) | 30 | 62˚54’ | 172˚04’ | 20 July | 10:35 | Day | 548.4 | 0 | 7 | 0 | 480.3 | 0 | 7 | 0 |
| | 22 (47) | 31 | 62˚35’ | 171˚26’ | 20 July | 18:45 | Day | 520.7 | 12 | 17 | 1 | 427.5 | 18 | 3 | 0 |
| | 23 (46) | 32 | 62˚10’ | 170˚30’ | 21 July | 1:10 | Night | 518.2 | 1 | 1 | 0 | 404.7 | 0 | 5 | 0 |
| | 23 (46) | 33 | 62˚10’ | 170˚30’ | 21 July | 10:55 | Day | 330.2 | 2 | 3 | 1 | 510.5 | 1 | 6 | 0 |
| | 24 (76) | 34 | 63˚00’ | 174˚05’ | 22 July | 1:30 | Night | 645.3 | 295 | 6 | 1 | 527.1 | 251 | 2 | 2 |
| 2018 | | | | | | | | | | | | | | | |
| | 4 (76) | 35 | 63˚09’ | 173˚50’ | 2 July | 14:08 | Day | 1144.5 | 3 | 2 | 0 | 928.4 | 3 | 3 | 0 |
| | 6 (56) | 36 | 62˚53’ | 172˚12’ | 3 July | 1:34 | Night | 875.9 | 44 | 0 | 5 | 928.1 | 94 | 0 | 13 |
| | 8 (36) | 37 | 62˚28’ | 170˚05’ | 3 July | 12:50 | Day | 515.9 | 56 | 3 | 0 | 334.1 | 31 | 0 | 0 |
| | 11 (55) | 38 | 63˚53’ | 172˚15’ | 4 July | 14:58 | Day | 794.8 | 1 | 0 | 0 | 750.9 | 2 | 0 | 0 |
| | 14 (46) | 39 | 64˚30’ | 170˚54’ | 5 July | 1:20 | Night | 704.3 | 1 | 0 | 0 | 646.8 | 0 | 0 | 0 |
| | 17 (35) | 40 | 64˚30’ | 168˚00’ | 5 July | 14:54 | Day | 279.9 | 10 | 0 | 0 | 487.6 | 33 | 0 | 0 |
| | 19 (28) | 41 | 64˚21’ | 166˚30’ | 5 July | 21:56 | Day | 294.7 | 0 | 0 | 0 | 247.6 | 0 | 0 | 0 |
| | 20 (45) | 42 | 65˚04’ | 168˚00’ | 6 July | 6:48 | Day | 512.0 | 11 | 0 | 0 | 656.3 | 15 | 0 | 0 |
| | 22 (52) | 43 | 65˚05’ | 169˚39’ | 6 July | 16:40 | Day | 588.7 | 6 | 0 | 0 | 392.4 | 2 | 0 | 0 |
| | 23 (49) | 44 | 65˚13’ | 169˚18’ | 7 July | 21:58 | Day | 711.0 | 39 | 0 | 0 | 706.5 | 91 | 0 | 0 |
| | 30 (42) | 45 | 66˚44’ | 168˚58’ | 11 July | 0:50 | Day | 652.9 | 14 | 0 | 0 | 475.6 | 17 | 0 | 0 |
| | 29 (56) | 46 | 66˚15’ | 168˚54’ | 11 July | 10:18 | Day | 575.4 | 10 | 0 | 0 | 571.8 | 22 | 0 | 0 |
| | 27r (46) | 47 | 65˚40’ | 168˚58’ | 11 July | 21:37 | Day | 397.1 | 59 | 0 | 0 | 619.5 | 51 | 0 | 0 |
| | 16r (41) | 48 | 64˚30’ | 169˚00’ | 12 July | 9:30 | Day | 305.4 | 164 | 0 | 0 | 244.7 | 36 | 0 | 0 |

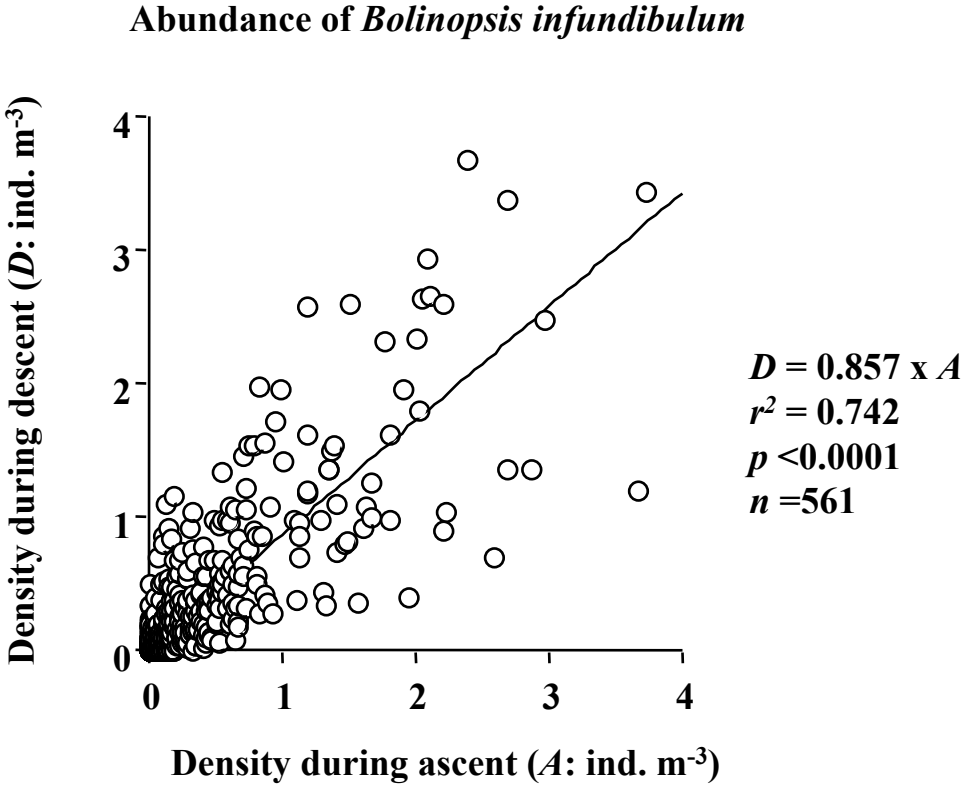


Appendix B. Scatter plot on the density of *Bolinopsis infundibulum* quantified during descent and ascent.

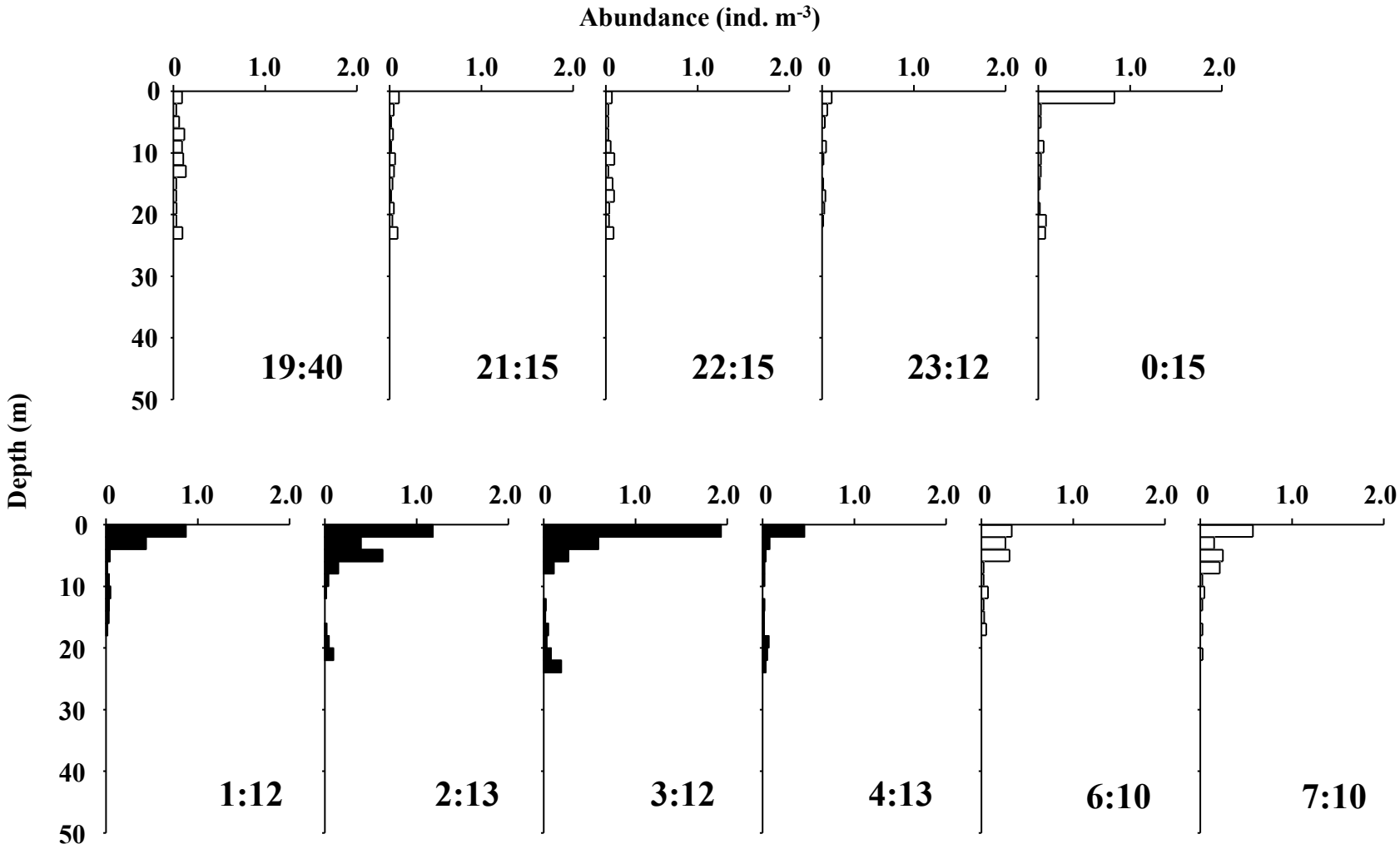


Appendix C. Diel changes in the vertical distribution of *Bolinopsis infundibulum* at St. 10 during 13–14 July 2017. Open and solid markers represent day and night, respectively.

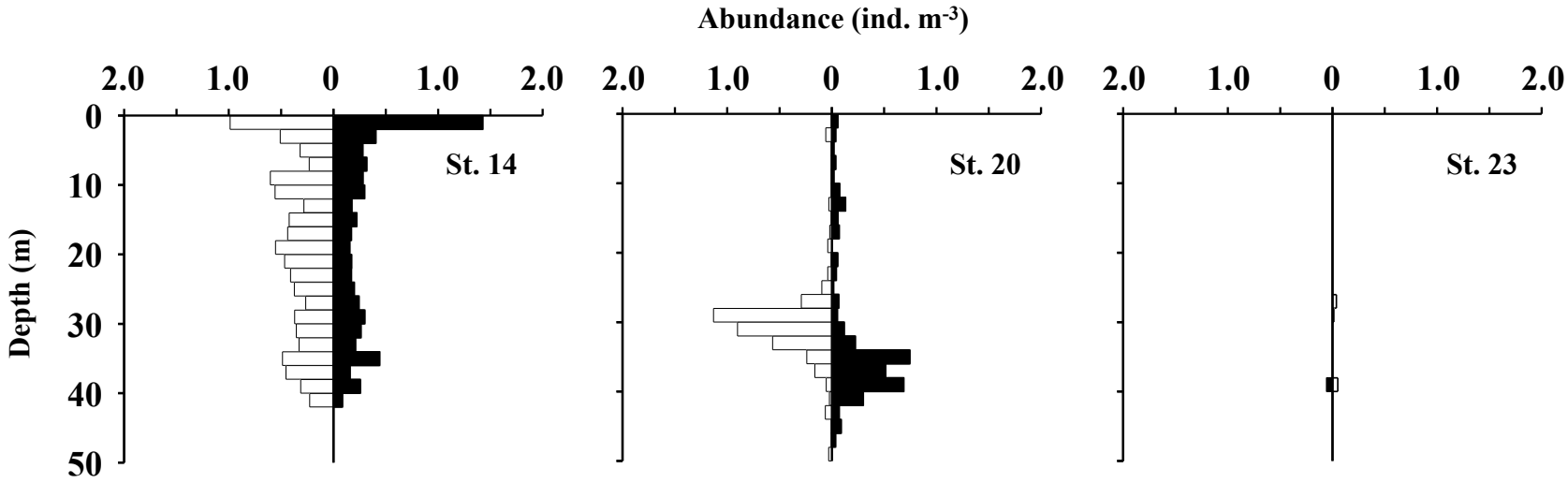


Appendix D. Day (open) and night (solid) vertical distribution of *Bolinopsis infundibulum* at St. 14, 20, 23 during 17–21 July 2017.

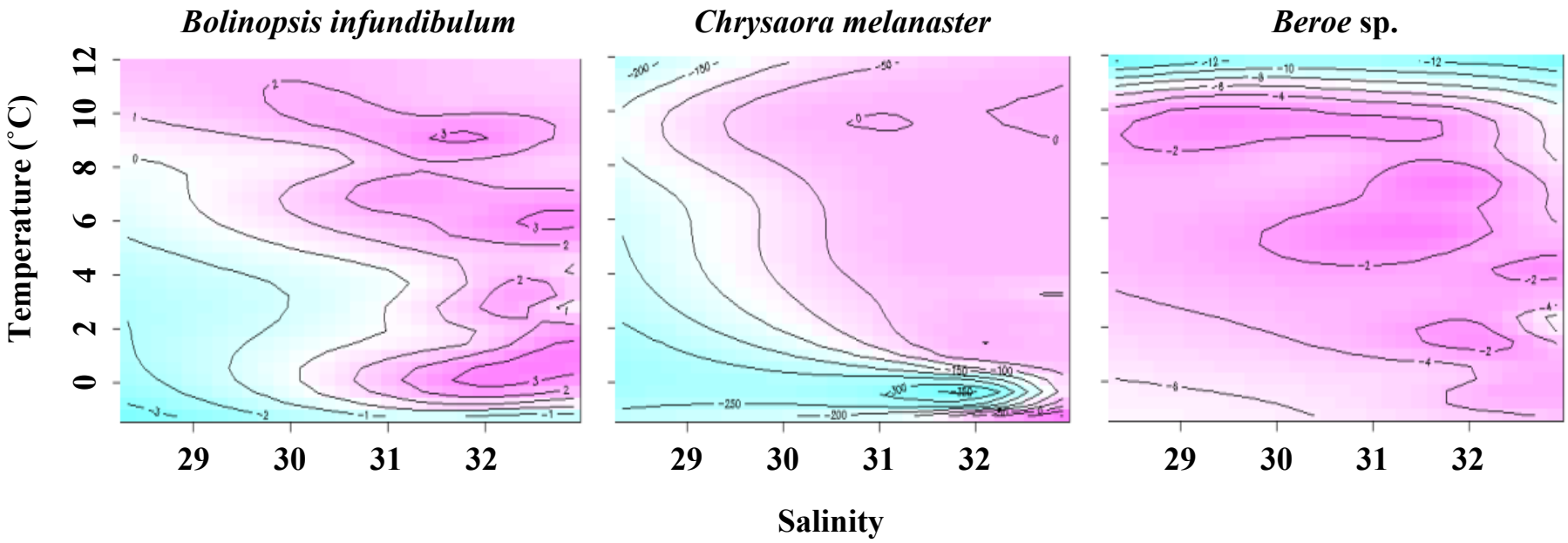


Appendix E. Contour plots for abundance anomalies of three large gelatinous zooplankton on a T-S diagram.

# Sea ice concentration

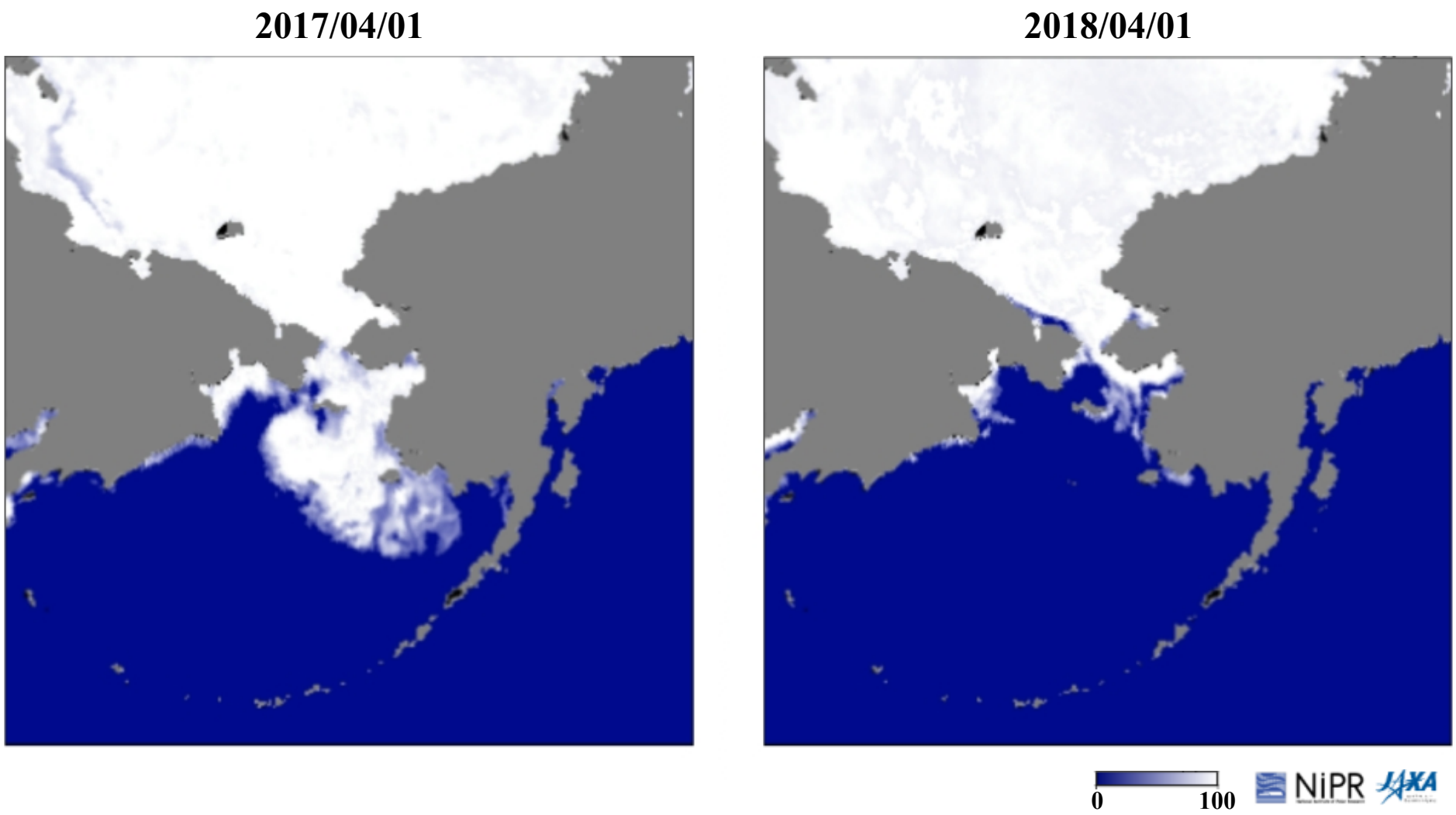


Appendix F. Sea ice concentration on April 1st in 2017 (left) and 2018 (right). Images were downloaded from Arctic Data archive System (ADS) (https://ads.nipr.ac.jp/).